Comparative Analysis of Interactive Modalities for Intuitive Endovascular Interventions

Wu, Di; Li, Zhen; Ansari, Mohammad Hasan Dad; Ha, Xuan Thao; Ourak, Mouloud; Dankelman, Jenny; Menciassi, Arianna; Momi, Elena De; Poorten, Emmanuel Vander

DOI
10.1109/TVCG.2024.3362628

Publication date
2025

Document Version
Final published version

Published in
IEEE Transactions on Visualization and Computer Graphics

Comparative Analysis of Interactive Modalities for Intuitive Endovascular Interventions

Di Wu, *Graduate Student Member, IEEE*, Zhen Li, *Member, IEEE*, Mohammad Hasan Dad Ansari, Xuan Thao Ha, Mouloud Ourak, Jenny Dankelman, *Member, IEEE*, Arianna Menciassi, *Fellow, IEEE*, Elena De Momi, *Senior Member, IEEE*, and Emmanuel Vander Poorten, *Member, IEEE*

***Abstract*—Endovascular intervention is a minimally invasive method for treating cardiovascular diseases. Although fluoroscopy, known for real-time catheter visualization, is commonly used, it exposes patients and physicians to ionizing radiation and lacks depth perception due to its 2D nature. To address these limitations, a study was conducted using teleoperation and 3D visualization techniques. This in-vitro study involved the use of a robotic catheter system and aimed to evaluate user performance through both subjective and objective measures. The focus was on determining the most effective modes of interaction. Three interactive modes for guiding robotic catheters were compared in the study: 1) Mode GM, using a gamepad for control and a standard 2D monitor for visual feedback; 2) Mode GH, with a gamepad for control and HoloLens providing 3D visualization; and 3) Mode HH, where HoloLens serves as both control input and visualization device. Mode GH outperformed other modalities in subjective metrics, except for mental demand. It exhibited a median tracking error of 4.72 mm, a median targeting error of 1.01 mm, a median duration of 82.34 s, and a median natural logarithm of dimensionless squared jerk of 40.38 in the in-vitro study. Mode GH showed 8.5%, 4.7%, 6.5%, and 3.9% improvements over Mode GM and 1.5%, 33.6%, 34.9%, and 8.1% over Mode HH for tracking error, targeting error, duration, and dimensionless squared jerk, respectively. To sum up, the user study emphasizes the potential benefits of employing HoloLens for enhanced 3D visualization in catheterization. The user study also illustrates the advantages of using a gamepad for catheter teleoperation, including user-friendliness and passive haptic feedback, compared to HoloLens. To further gauge the potential of using a more traditional joystick as a control input device, an additional study utilizing the Haption Virtuose robot was conducted. It reveals the potential for achieving smoother trajectories, with a 38.9% reduction in total path length compared to a gamepad, potentially due to its larger range of motion and single-handed control.**

***Index Terms*—Augmented reality, catheter navigation, endovascular intervention, robotic catheter, user study.**

Manuscript received 24 July 2023; revised 24 January 2024; accepted 28 January 2024. Date of publication 6 February 2024; date of current version 3 January 2025. This work was supported in part by the ATLAS project. This work was supported in part by the European Union's Horizon 2020 research and innovation programme under the Marie Sklodowska-Curie under Grant 813782. This work was also supported in part by the European Union's Horizon 2020 research and innovation programme under Grant 101017140, in part by the ARTERY project. Moreover, this research was funded in part by the Postdoctoral Mandates (PDM), an internal fund of KU Leuven under Grant 3E230593, and in part by the CURE project, another internal KU Leuven fund, with under grant 3E210658. Recommended for acceptance by L. Wang. *(Di Wu and Zhen Li contributed equally to the implementation and writing of this work and are designated as co-first authors.) (Corresponding author: Zhen Li.)*

This work involved human subjects or animals in its research. The author(s) confirm(s) that all human/animal subject research procedures and protocols are exempt from review board approval.

Di Wu is with the Department of Mechanical Engineering, KU Leuven, 3000 Leuven, Belgium, and also with the Faculty of 3mE, Delft University of Technology, 2628CD Delft, The Netherlands (e-mail: di.wu@kuleuven.be).

Zhen Li is with the Department of Electronics, Information and Bioengineering, Politecnico di Milano, 20133 Milano, Italy, and also with the Faculty of 3mE, Delft University of Technology, 2628CD Delft, The Netherlands (e-mail: zhen.li@polimi.it).

Mohammad Hasan Dad Ansari and Xuan Thao Ha are with the Department of Mechanical Engineering, KU Leuven, 3000 Leuven, Belgium, also with The BioRobotics Institute, Scuola Superiore Sant'Anna, 56127 Pisa, Italy, and also with the Department of Excellence in Robotics & AI, Scuola Superiore Sant'Anna, 56127 Pisa, Italy (e-mail: hasan.mohammad@santannapisa.it; xuanthao.ha@kuleuven.be).

Mouloud Ourak and Emmanuel Vander Poorten are with the Department of Mechanical Engineering, KU Leuven, 3000 Leuven, Belgium (e-mail: mouloud.ourak@kuleuven.be; emmanuel.vanderpoorten@kuleuven.be).

Jenny Dankelman is with the Faculty of 3mE, Delft University of Technology, 2628CD Delft, The Netherlands (e-mail: j.dankelman@tudelft.nl).

Arianna Menciassi is with The BioRobotics Institute, Scuola Superiore Sant'Anna, 56127 Pisa, Italy, and also with the Department of Excellence in Robotics & AI, Scuola Superiore Sant'Anna, 56127 Pisa, Italy (e-mail: arianna.menciassi@santannapisa.it).

Elena De Momi is with the Department of Electronics, Information and Bioengineering, Politecnico di Milano, 20133 Milano, Italy (e-mail: elena.demomi@polimi.it).

This article has supplementary downloadable material available at https://doi.org/10.1109/TVCG.2024.3362628, provided by the authors.

Digital Object Identifier 10.1109/TVCG.2024.3362628

I. Introduction

ENDOVASCULAR intervention is a minimally invasive interventional procedure for treating various cardiovascular diseases. It involves the insertion of one or more slender, flexible catheters into a blood vessel, allowing physicians to access the heart and surrounding vasculature for diagnostic or therapeutic purposes. Compared to conventional open-heart surgery, catheterization is less invasive, requiring only a small incision for catheter insertion [1]. This reduces the risk of complications, shortens recovery time, and leaves minimal scarring [2], thus gaining wide applications.

Throughout the procedure, physicians can employ real-time imaging techniques, such as fluoroscopy, to visualize the heart and blood vessels [7], [8]. This facilitates the identification of lesions, the navigation itself, as well as the immediate evaluation of treatment effectiveness. However, fluoroscopy exposes both patients and physicians to ionizing radiation. In particular, physicians who are repeatedly exposed to radiation face a higher risk of cancer and cataracts [9]. Furthermore, the two-dimensional (2D) nature of fluoroscopic images prevents depth perception [10], [11], complicating the precise maneuvering of catheters within intricate vessels.

One approach to tackle the challenges mentioned above is 3D imaging and visualization. A variety of methods have been used to produce a 3D model of the vessel. Some groups employ 3D rotational angiography [12]. Others propose to fuse the pre-acquired 3D images (e.g., from Computed Tomography (CT) or Magnetic Resonance Imaging (MRI)) with real-time fluoroscopy [10], [13]. These methods can provide improved depth information, yet radiation exposure still remains a concern. Non-radiative imaging modalities, e.g., Optical Coherence Tomography (OCT) [14] and IntraVascular UltraSound (IVUS) [15], could also be employed to produce some sort of depth information during catheter-based procedures. By utilizing the aforementioned techniques, 3D reconstruction of 2D medical images could be made available. However, the optimal use of this 3D content still requires further investigation. Displaying these 3D volumetric data on a 2D screen is a cheap and common method. However, 2D screens do not manage to convey the third dimension very well [16]. Moreover, 2D screens hinder direct interaction with the image [17]. Augmented Reality (AR) systems present an appealing alternative interface by overlaying 3D rendered images onto the physician's field of view during the procedure. This technology could improve depth perception and spatial understanding, facilitating more accurate instrument placement and navigation [18]. It should be noted that while many 3D reconstruction methods have been introduced previously, the primary objective of this study is to investigate the optimal presentation of the 3D content, with different display techniques, rather than investigating intra-operative 3D reconstruction methods themselves.

Along these lines, an image guidance system using AR visualization is proposed for transcatheter procedures in [3]. The 3D hologram displayed in AR was the pre-operative 3D model reconstructed from CT scans. The catheter tip position is derived from the 2D segmentation of intra-operative fluoroscopy images and registered to the 3D model. Although this method improves visualization, radiation exposure from fluoroscopy remains a concern. Palumbo et al. explored the use of AR for radiation-free catheter navigation [4]. In their work, the guidewire's tip pose is determined by Electromagnetic (EM) trackers. However, their work only introduced a registration method that aligns the EM tracker position with a holographic marker. Guidewire or vessel phantoms were not used to investigate in detail the influence of AR on vessel navigation. A related approach is presented in [5] for Endovascular Aortic Repair (EVAR), where the catheter tip position is also obtained using an EM tracker. This work merely represents the tip position as a sphere. This representation neglects the orientation of the tip, which is crucial for assessing whether the catheter is in a hazardous pose. Furthermore, the paper only describes the concept and implementation without providing any quantitative results regarding the effectiveness of assistance offered by AR visualization.

Linte et al. achieved catheter tip visualization in AR through ultrasound imaging [6]. The work assessed the effectiveness of AR visualization by having three novices use a commercial cable-driven manual catheter to target four specific locations within a heart phantom. The results indicate that AR visualization could enhance targeting accuracy when compared to 2D ultrasound images, while the assistance provided by AR in vascular navigation is yet to be validated. Apart from the limitations mentioned above, physicians may need training and time to become comfortable with AR systems, and extra research is needed to come to an optimal integration of AR into the clinical workflow. In addition to prior studies, the effectiveness of AR visualization for showing hidden anatomical structures has also been validated in the field of neurosurgery [19].

Besides AR, Virtual Reality (VR) has also been employed in surgical training for personalized Percutaneous Coronary Intervention (PCI) [20]. However, the VR-based simulators developed for this purpose are limited to pre-operative training and rehearsal. The simulator cannot be utilized during intra-operative procedures. The choice for AR over VR in this study is primarily due to AR's suitability for intra-operative use. AR's "see-through" feature allows interventionists to maintain visibility of the actual operating environment [21], a critical factor for patient safety and effective procedure execution. Additionally, AR can be smoothly integrated into the existing setup of a catheterization lab without extensive digital reconstruction of the environment. AR also offers improved efficiency when interacting with virtual objects compared to VR, owing to a more direct understanding of spatial relationships [22]. Furthermore, AR tends to cause less disorientation and discomfort [22], which are sometimes associated with VR use.

Upon a review of the previous literature as summarized in Table I, it was found that no studies investigated the potential of using AR for endovascular interventions with robotic catheters in an in-vitro study. A possible explanation for the lack of such studies is the limited availability of robotic catheter platforms, the recent availability of high-quality AR Head-Mounted Display (HMD), and the complexity of integrating all these components.

Teleoperated catheter navigation can also significantly reduce radiation exposure [23]. This technology could also potentially allow physicians to perform intricate procedures with enhanced precision and reduced physical strain. Teleoperation can be accomplished using a variety of control input devices. Researchers have explored the use of joystick-like controllers [24], [25], haptic devices [26], and custom-made input devices [27] for teleoperating catheters. The user-friendly nature and widespread familiarity with joystick-like controllers can facilitate a smoother transition from gaming to interventions and a shorter learning time for physicians using teleoperated catheter systems. Subsequently, this can result in increased procedural efficiency, patient safety, and better outcomes. The custom-made input device designed in [27] consists of a tube and several sensors, resembling a catheter. This allows physicians to manipulate the input device more intuitively using familiar actions such as rotation and pushing, similar to how they would handle a catheter in current practice.

This work presents a user study investigating the effects of different interactive modalities in human-in-the-loop robot-assisted endovascular interventions. In this study, two visualization methods for 3D content are investigated: 1) a standard 2D monitor and 2) an advanced 3D visualization technique using AR. One aim of this work is to determine which visualization

TABLE I
COMPARISON WITH PREVIOUS WORK

References	Procedure	Device	Manual/Motorized catheter delivering	AR device	Intraoperative feedback on catheter pose	Evaluation methods	Validation through vessel navigation
[3] Liu et al.	transseptal puncture	Destino™ Reach catheter	manual	HoloLens	dual fluoroscopic images	image registration accuracy	yes, 1 user
[4] Palumbo et al.	structural interventional cardiology	guidewire	manual	HoloLens 2	EM tracking system	registration accuracy	no
[5] Garcia et al.	endovascular aneurysm repair	stent graft catheter	manual	HoloLens	EM tracking system	system feasibility	yes but no quantitative evauation
[6] Linte et al.	atrial ablation	Freezor™ catheter	manual	2D monitor	ultrasound images and EM tracking system	targeting accuracy	yes, 3 users
This work	endovascular interventions	custom-made robotic catheter	motorized, teleoperation with four modes	HoloLens 2	EM tracking system	tracking, targeting accuracy + NASA-TLX	yes, 15 users

approach is more effective at this stage in a first in-vitro study. The other aim of this work is to primarily compare the use of a gamepad and an HMD as input devices. To the best of the authors' knowledge, this is the first time that an HMD has been utilized as a control input device for catheter steering. The main contributions of this work are:

- design of an AR interface in HMD for enhanced visual feedback and catheter steering, implementing gamepad-based teleoperation to steer a robotic catheter system, integrating stand-alone components such as a robotic catheter, catheter driver, HMD and gamepad into a complete robotic catheter system;
- in-vitro user study with various combinations of control and visualization devices, involving fifteen participants with diverse levels of experience in HMD, gaming, and steerable catheters;
- a detailed performance analysis and discussion comparing the different interactive modalities;
- an additional in-vitro study with a haptic device that has a larger range of motion as the control input device and an HMD for visualization.

The paper is organized as follows: Section II provides an overview of the hardware components used in the system and their integration. Section III explains the experimental design and the performance metrics employed to evaluate the efficacy of catheter navigation. Section IV showcases the results, accompanied by a discussion. Section V features an additional study employing a Haption Virtuose robot as the control input device. The Virtuose offers a broader range of motion compared to a gamepad and allows coordination of catheter motion with a single hand thanks to its six Degrees of Freedom (DoFs). Section VI offers conclusions and outlines future work.

II. EXPERIMENTAL SETUP AND METHODOLOGY

A. System Components

To investigate various interactive modalities for catheter navigation, an experimental setup for endovascular interventions was developed (as shown in Fig. 1). It consists of the following components:

a) Silicone Aortic Phantom: the aortic phantom (T-S-N-002, Elastrat Sarl, Geneva, Switzerland) is made of silicone, and hence deformable. The wall thickness has been chosen such that deformations correspond to the deformations one expects in a real vessel. The phantom replicates key anatomical features such as the descending aorta, aortic arch, aortic root, and coronary arteries.

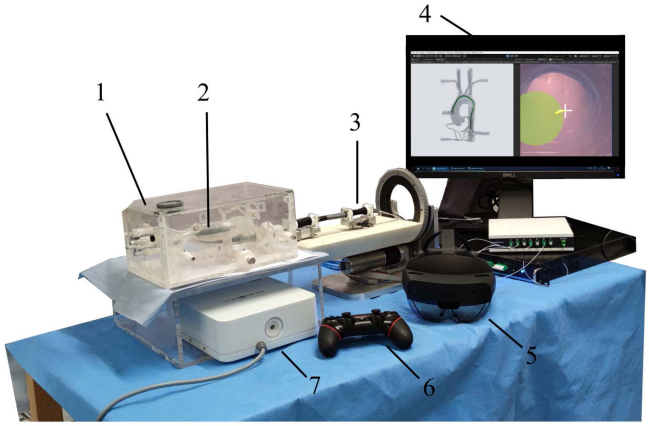

Fig. 1. Experimental setup for in-vitro user study: 1. silicone aortic phantom; 2. pneumatically-driven robotic catheter; 3. catheter driver; 4. standard 2D monitor; 5. Head-Mounted Display (HMD); 6. wireless gamepad; 7. electromagnetic field generator.

b) Robotic Catheter: an in-house developed robotic catheter with a 50 mm bendable Nitinol segment, outfitted with a pattern of equally spaced slots produced by Electrical Discharge Machining (EDM). These slots make the segment bendable. The remaining section, approximately 1 m in length, is composed of a predominantly passive flexible plastic tube. With a diameter of 7 mm, the catheter is well suited for navigation within the aorta, as the typical diameter of the aorta ranges between 20 and 35 mm [28]. The bendable Nitinol segment of the robotic catheter features four Pneumatic Artificial Muscles (PAMs), organized into two antagonistic pairs [29]. Each PAM has one end connected off-center to the catheter tip. When pressure is applied to the muscle, its length decreases, generating a pulling force on the catheter tip, forcing it to bend. By concurrently controlling two antagonistic pairs of the PAMs, the catheter achieves a spatial 2-DoF bending motion. A 6-DoF EM sensor (Aurora®, Northern Digital Inc., Canada) is glued to the center of the catheter tip, enabling precise tip localization.

c) Catheter Driver: the catheter driver [30] is designed for axial rotation about the catheter's longitudinal axis and for 1-DoF insertion or retraction of the catheter. The device relies on two sleeve-based grippers. One end of the sleeve remains

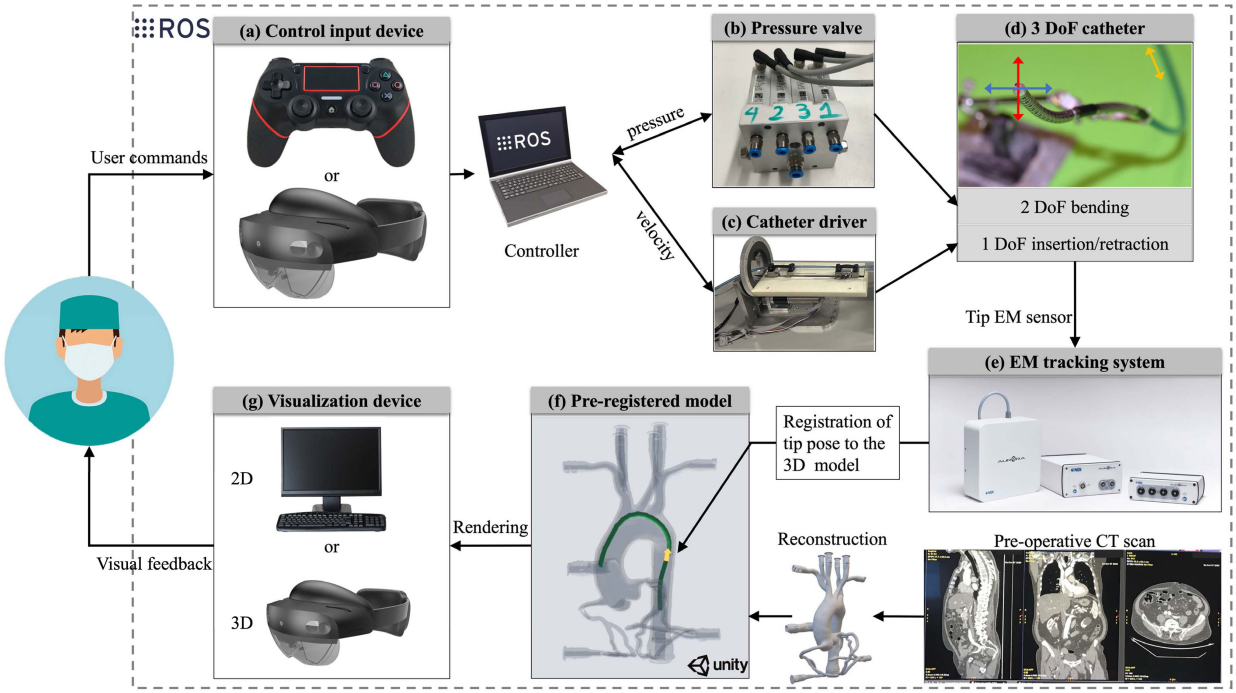

Fig. 2. Schematic of the advanced human-in-the-loop vessel navigation system with multiple interactive modalities, including: (a) a gamepad or an HMD as control devices; (b) a pneumatic valve with four output ports receives control commands from ROS; (c) the catheter driver, operated through velocity control, regulates the insertion and retraction of the catheter; (d) the PAM-driven catheter, having 2-DoF and a 50 mm active bendable segment; (e) an EM tracking system localizing the catheter tip, whose pose is then registered to the mesh frame of the 3D reconstructed model; (f) the virtual 3D aortic model reconstructed utilizing high-resolution CT images, along with the guidance path and the catheter tip pose registered and rendered in this virtual model frame; (g) visual feedback that users receive either through a standard monitor (2D) or via a HoloLens (3D).

stationary, while the other end is attached to a pneumatic piston. As pressure increases, the sleeve expands in length, subsequently reducing its diameter and ensuring a firm grip on the catheter body. The two grippers operate alternately, with one gripping as the other releases. This synchronized operation allows for continuous catheter translation over a large stroke.

d) Head-Mounted Display (HMD): Microsoft HoloLens 2, simply referred to as "HoloLens" in the following, is an advanced AR HMD featuring 3D visualization. Its advanced display technology projects holograms, which are 3D virtual objects, into the user's field of view. These holograms blend seamlessly with the real world. The HoloLens also has sophisticated hand-tracking capabilities for both hands. The HoloLens hand-tracking system enables smooth interactions for users, allowing them to select and position holograms using direct touch, as if interacting with tangible objects in the real-world space. Moreover, the hand-rays originating from the user's palm center serve as an extension of their hand, enabling seamless interaction with holograms that are beyond physical reach. The wireless design of the HoloLens promotes unlimited movement without the burden of external cables. Voice control is another feature of the HoloLens. Despite its advanced features, the HoloLens weighs only 3.28 kg.

e) Gamepad: the controller (Yues, Dublin, Ireland) is a wireless input device for gaming. The controller is equipped with four buttons on the left, two central thumbsticks, and four additional buttons on the right.

f) Electromagnetic Field Generator: an EM field generator (Northern Digital Inc., Canada) is placed beneath the phantom. When the EM sensor enters the electromagnetic field produced by the field generator, it induces a small current within the sensor. This current is then converted into the corresponding positions and orientations of the EM sensor. However, the presence of electromagnetic materials within this field tends to distort the accuracy of these measurements. For this reason, the catheter driver's metal components are located outside the generated magnetic field so as not to disturb it. The 6-DoF EM sensor embedded in the catheter tip allows tip pose measurement at 40 Hz.

g) Software Architecture: communication between various devices is facilitated through ROS 1 [31], with each device functioning as a distinct node within the system. The 3D content displayed on both the 2D monitor and HMD is rendered using the Unity3D game engine [32].

Fig. 2 presents the control schematic for human-in-the-loop catheter navigation with visual feedback. Users can interact with either a gamepad or a HoloLens to generate control commands, while obtaining 3D visual feedback from a HoloLens or 2D visual feedback from a standard 2D screen.

B. System Integration and User Interface Design

This subsection explains how the different parts are integrated into a catheterization system and describes the design of the user interface.

The functionalities of the various thumbsticks or buttons are illustrated in Fig. 3(a). By using a ROS joystick driver library, the bending angle of the thumbstick can be read as a float value

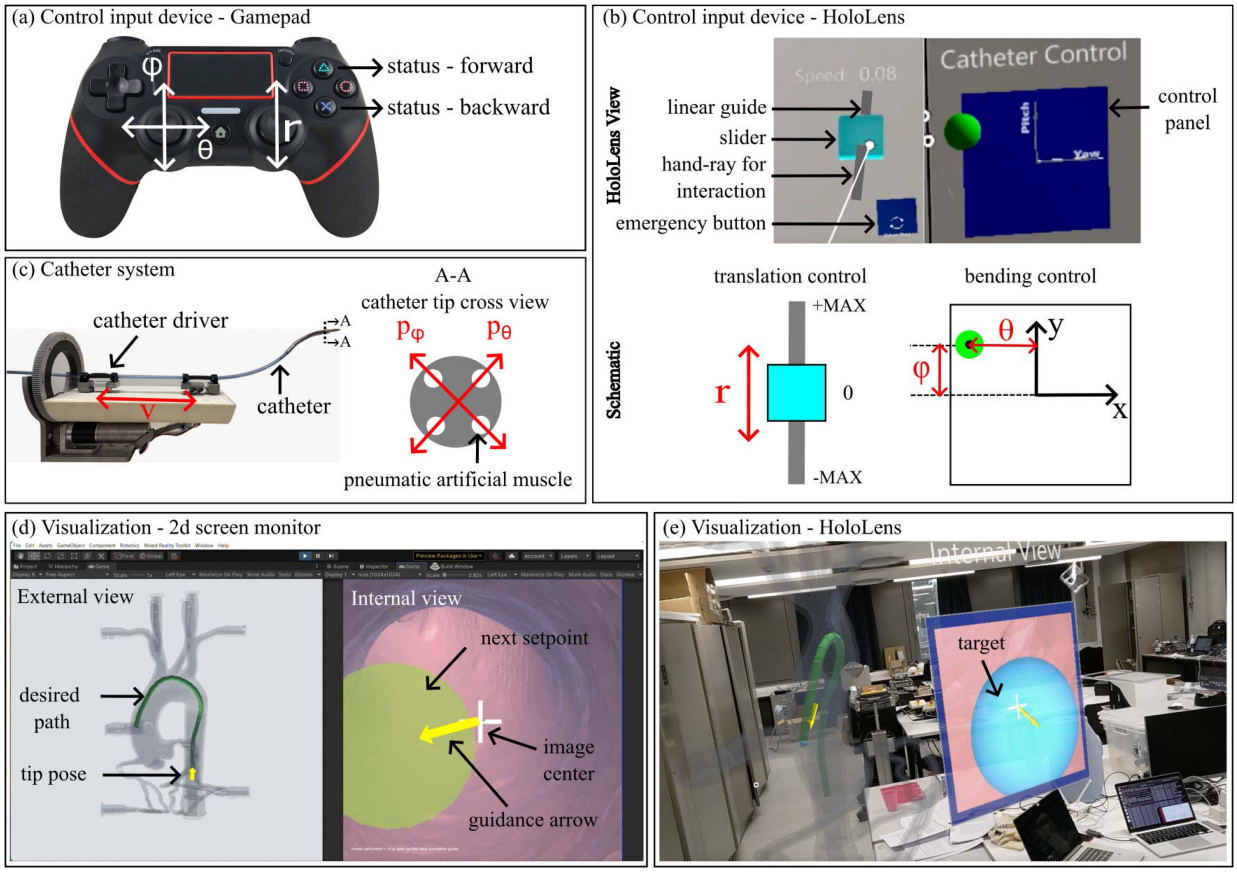

Fig. 3. User interfaces for input devices and visual feedback: (a) a gamepad as a control input device; (b) a HoloLens serves as a control input device, featuring hand gesture recognition capabilities; (c) a schematic illustration outlining the three mapping relationships corresponding to the 3-DoF for the catheter system; (d) 2D visualization using standard monitor; (e) 3D visualization using HoloLens: Users can view the holograms from various angles by physically moving around in real-world space.

between 0 and 1, while the button toggles between two distinct values: 0 and 1. Users can control the 2-DoF bending by directly mapping the bending angle of the left thumbstick (ϕ, θ) to the pressure applied to the PAMs (p_ϕ, p_θ), namely p_ϕ is proportional to ϕ, and p_θ is proportional to θ. The maximum pressure applied to PAMs is set at 6 bar. The right thumbstick is employed to regulate the catheter driver's insertion/retraction motion speed. The catheter driver is operated using velocity control. The thumbstick's bending angle r is mapped to the translation speed of the catheter driver v, namely v is proportional to r. The maximum translational speed was set to 5 mm/s. To prevent excessively rapid changes in the catheter's motion direction, e.g., when releasing the thumbstick, which, equipped with a return spring would quickly oscillate back and forth around the neutral position, the motion direction is explicitly indicated by a button. The PS (Δ) and OPTIONS (X) buttons on the right (refer to Fig. 3(a)) are used to indicate forward and backward motion respectively as in:

$$v \propto \begin{cases} \beta r & \text{if } r > 0 \\ 0 & \text{if } r \leq 0 \end{cases} \text{and } \beta = \begin{cases} 1 & \text{if PS}(\Delta) \\ -1 & \text{if OPTIONS(X)} \end{cases} \quad (1)$$

The method of consciously selecting between movement directions is adopted as an alternative to the establishment of a deadzone where the catheter driver's speed defaults to zero. It may be worth comparing both methods in future user trials.

Fig. 3(b) illustrates the user interface design of the HoloLens when used as a control input device. Users can send control commands for steering the catheter by engaging with virtual buttons or sliders shown by the HoloLens in a manner akin to interacting with actual objects. The speed, v, of the catheter driver is regulated by the translational distance of the slider, r. An emergency button has been incorporated to allow users to quickly stop the catheter's translational movement in case of an emergency. In the blue square control panel shown on the right, a green sphere can be moved on this 2D plane. The sphere's coordinates are measured and proportionally converted into pressures. These pressures are then transmitted to the PAMs in two orthogonal directions, denoted as p_ϕ and p_θ. Users can reposition various holographic components in the HoloLens view by grasping and dragging them, allowing them to customize the layout to their optimal comfort level. Moreover, users can engage a hand-ray, a common remote control feature in HoloLens, that extends from their palm towards the holographic object. This allows them to interact with the holographic object even when the object is situated beyond their physical reach.

Control commands generated by the gamepad or HoloLens are sent to the pressure valves, which adjust catheter bending,

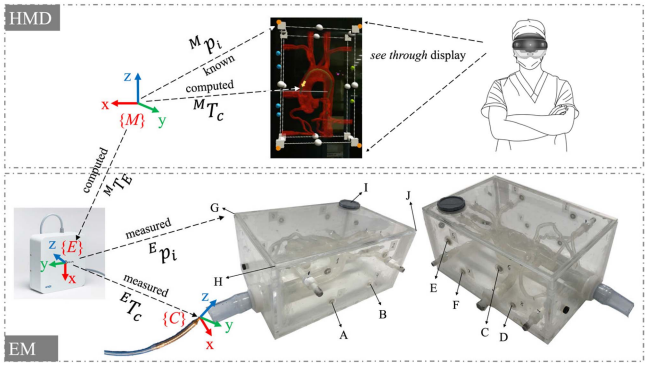

Fig. 4. Visualization of ten markers (A-J) located on different surfaces of the phantom's outer casing, along with the coordinate frames used in the registration process. The transformations ${}^{M}\boldsymbol{T_E}$ achieved through registration and ${}^{E}\boldsymbol{T_C}$ obtained from EM measurements enable precise representation of the tip's position in the mesh frame $\{\boldsymbol{M}\}$.

and to the catheter driver, which manages the catheter's translational movement, as shown in Fig. 3(c). This process allows for precise control over the robotic catheter's 3-DoF.

An EM tracker, affixed to the catheter tip, captures its pose within the magnetic field created by an EM field generator. The tip pose is expressed through the transformation matrix ${}^{E}\boldsymbol{T_C}$ that registers the tip frame $\{\boldsymbol{C}\}$ to the EM frame $\{\boldsymbol{E}\}$, with ${}^{E}\boldsymbol{T_C}$ determined through EM measurement. A 3D aortic mesh model is reconstructed from CT images. To represent the catheter pose correctly in the aortic model frame $\{\boldsymbol{M}\}$, the transformation matrix ${}^{M}\boldsymbol{T_C}$ is needed and is calculated as follows:

$$ {}^{M}\boldsymbol{T_C} = {}^{M}\boldsymbol{T_E}\,{}^{E}\boldsymbol{T_C} = \begin{bmatrix} \boldsymbol{R} & \boldsymbol{t} \\ \boldsymbol{0} & 1 \end{bmatrix} {}^{E}\boldsymbol{T_C} \tag{2} $$

Ten markers are employed to calculate the transformation matrix ${}^{M}\boldsymbol{T_E}$ that registers the EM frame $\{\boldsymbol{E}\}$ to the virtual mesh model frame $\{\boldsymbol{M}\}$. These markers are strategically positioned on the outer casing of the silicone aortic phantom (refer to Fig. 4). Two datasets are involved in this process: one comprises the positions of the ten markers ${}^{M}\boldsymbol{p} = \{{}^{M}\boldsymbol{p}_i, i = 1, 2, \ldots, m\}$ within the virtual model frame $\{\boldsymbol{M}\}$, and the other contains the positions ${}^{E}\boldsymbol{p} = \{{}^{E}\boldsymbol{p}_i, i = 1, 2, \ldots, m\}$ of the ten markers represented in the EM frame $\{\boldsymbol{E}\}$, where $m = 10$.

The optimal transformation matrix ${}^{M}\boldsymbol{T_E}$ is determined through a Singular Value Decomposition (SVD) method [33] following the steps as shown in Table II. The objective function is defined as follows:

$$ \min_{{}^{M}\boldsymbol{T_E}} f = \sum_{i=1}^{m} \left|\left| {}^{M}\boldsymbol{p}_i - {}^{M}\boldsymbol{T_E}\,{}^{E}\boldsymbol{p}_i \right|\right|^2 \tag{3} $$

The Root Mean Square Error (RMSE), as defined by (4), was calculated based on the ten registration markers.

$$ RMSE = \sqrt{\frac{\sum_{i=1}^{m} \left|\left| {}^{M}\boldsymbol{p}_i - {}^{M}\boldsymbol{T_E}\,{}^{E}\boldsymbol{p}_i \right|\right|^2}{m}} \tag{4} $$

In our study, seven registration procedures were implemented. The recorded errors for these seven registrations were 4.68 mm, 4.87 mm, 4.53 mm, 4.61 mm, 4.54 mm, 4.62 mm, and 5.36 mm. The registration error primarily stems from the discrepancies between the phantom and the model, attributed to manufacturing inaccuracies and the aging of the silicon phantom due to wear and tear. A secondary source of error arises from the measurement inaccuracies inherent to the EM sensors. After the registration process, the virtual mesh model along with the representation of the catheter tip pose is visualized either on a conventional 2D monitor or through a HoloLens.

TABLE II
STEPS TO DETERMINE THE OPTIMAL TRANSFORMATION MATRIX USING A SVD METHOD

Step	Description
1	**Centroid Calculation:** Compute the centroids of datasets ${}^{E}\boldsymbol{p}$ and ${}^{M}\boldsymbol{p}$. Denote them as $\boldsymbol{c_E}$ and $\boldsymbol{c_M}$, respectively.
2	**Demean the Datasets:** Translate each dataset by subtracting its centroid. Using the equations: ${}^{E}\boldsymbol{p'} = {}^{E}\boldsymbol{p} - \boldsymbol{c_E}$, ${}^{M}\boldsymbol{p'} = {}^{M}\boldsymbol{p} - \boldsymbol{c_M}$
3	**Compute Cross-Covariance Matrix:** Calculate H as: $H = {}^{E}\boldsymbol{p'}^{T}\,{}^{M}\boldsymbol{p'}$.
4	**Singular Value Decomposition (SVD):** Decompose the matrix H using SVD. This results in three matrices: U (left singular vectors), S (diagonal matrix of singular values), and V^T (right singular vectors). So, $H = USV^T$.
5	**Compute Rotation Matrix:** Calculate the rotation matrix R as: $R = VU^T$.
6	**Handle Reflection Case:** If det(R) is -1, correct R by multiplying the last column of U by -1.
7	**Compute Translation Vector:** Compute t as: $t = \boldsymbol{c_M} - R\,\boldsymbol{c_E}$.
8	**Final Transformation:** Apply R and t to align ${}^{E}\boldsymbol{p}$ with ${}^{M}\boldsymbol{p}$. Denote result as ${}^{M}T_E$.

The visualizations for both standard 2D monitor and HoloLens can be seen in Fig. 3(d) and (e), respectively, each showcasing similar user interface designs. The user interface is divided into two sections: an external view on the left and an internal view on the right. The external view presents a comprehensive perspective of the aorta, with a thick green line illustrating the desired path for users to follow and a yellow arrow indicating the current pose of the catheter tip. The internal view offers an inside-the-vessel, forward-looking perspective akin to angioscopy. Within this view, several discrete green spheres indicate the path setpoints. Specifically, there are 26 green spheres representing the 26 setpoints derived from the path planning algorithm. The green spheres are not uniformly distributed along the aorta. Their placement is determined by the path planning algorithm that takes various constraints into account. The path planning method is further elaborated in the following paragraph. A yellow guidance arrow is added to indicate the direction and degree to which the catheter tip should bend from the current position. The white cross represents the center of the field of view. A blue sphere represents the final target at the end of the path that users must aim to reach as accurately as possible.

The desired path of the catheter is generated through a derivative Reinforcement Learning (RL) method based on the approach outlined in reference [34]. This method is employed to ensure the optimality of the path and the fulfillment of robotic catheter constraints. The reward function of the RL algorithm

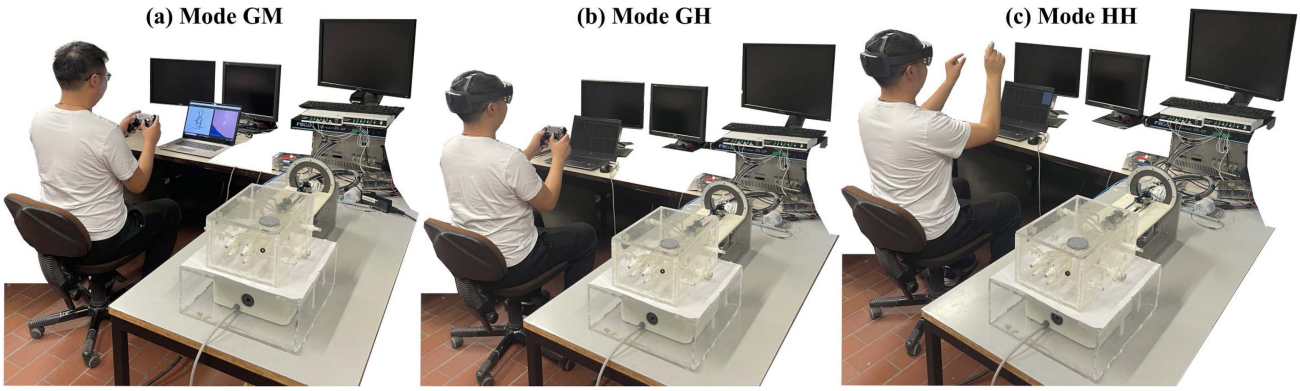

Fig. 5. Three interactive modalities investigated in this work, with their control devices and visualization devices outlined in Table III.

TABLE III
THREE INTERACTIVE MODALITIES INVESTIGATED IN THIS WORK

	control devices	visualization devices
Mode GM	Gamepad (G)	2D monitor (M)
Mode GH	Gamepad (G)	HoloLens (H)
Mode HH	HoloLens (H)	HoloLens (H)

takes into account several criteria: the number of steps (negative reward "-"), the number of collisions (-), whether the target position is reached (positive reward "+"), whether a path setpoint is close to the centerline (+), and whether the bending angle of the catheters is sufficient to navigate a trajectory's curvature while staying within its bending capacity (+).

It should be noted that the internal view is not present in current clinical practice. In this work, the internal view serves as an innovative feature for enhancing navigation capabilities within the vessels. The internal view images are captured through a virtual camera in Unity3D. The pose of the camera is continuously synchronized with the catheter tip pose, offering the operator a first-person view. In future clinical practice, the internal view could be reconstructed from IVUS or OCT images.

III. EXPERIMENTAL PROTOCOL

A. Experimental Procedure

In this study, two input devices (gamepad and HoloLens) and two visualization techniques (HoloLens and 2D monitor) are investigated. The combinations of these control devices and visualization techniques could yield four possible interactive modalities. Using the HoloLens solely as a control device without offering visualization makes little sense and underutilizes its potential, as it is primarily considered an enhanced visualization tool, with control functionality as a secondary feature. Consequently, we concentrate on the remaining three interactive modalities, as outlined in Table III with corresponding experimental setup presented in Fig. 5. Mode GM denotes the use of a gamepad (G) as the control input device and a 2D monitor (M) for visualization. Mode GH denotes the use of a gamepad (G) as the control input device and the HoloLens (H) for visualization. Mode HH denotes the use of the HoloLens (H) both as the control input device and for visualization. The experimental procedure is as follows:

1. participants are asked whether they are interested in participating in this study and if so, are asked to complete an informed consent form based on the standard format provided by KU Leuven [35]. The following information is communicated to the participants: the specific tasks, namely navigating catheters in the aortic phantom, the assurance that the experiment will not involve the collection of any personal information, and their right to discontinue the experiment at any time without providing a reason.
2. the hardware, techniques, and experimental procedures are clearly explained to the participants.
3. each participant is allotted a total of 10 minutes to familiarize him(her)self with the system and its three interactive modes.
4. participants complete three trials for each mode, advancing to the next mode only after finishing the current one. The order of the modes varies among users: five participants adopt the sequence Mode GM-GH-HH, another five engage in Mode GH-HH-GM, while the remaining five progress through Mode HH-GM-GH. Due to practical considerations, three types of order are employed instead of six. By changing the order of the modes, the potential impact of the learning curve is distributed across all modes, making it less likely that the learning effect biases the results. In total, each user performs nine trials. The specific details of a trial are described in Section III-B.
5. upon completion of the three trials per mode, participants are asked to fill out a NASA Task Load Index (NASA-TLX) form [36]. Once the participants have completed all nine trials, they are requested to complete an additional tailor-made questionnaire.

The NASA-TLX form assesses user workload on a 20-point scale using six metrics: mental demand, physical demand, temporal demand, performance, effort, and frustration. Participants rated each mode based on these dimensions by considering task-related aspects: 1) How mentally demanding was the task? 2) How physically demanding was the task? 3) To what extent did you feel a sense of urgency or haste in the task's pacing? 4) How successful were you in completing the task? 5) How much effort

did you spend to achieve your performance level? 6) To what extent did one feel insecure, discouraged, irritated, stressed, or annoyed? The tailor-made questionnaire also collected data on participants' profession, eyewear usage, dominant hand, prior gaming and HoloLens experience, and their good/bad experiences during the experiment.

B. Task Details for a Single Trial

The aim of each experiment is to steer a robotic catheter within an aortic phantom from the descending aorta to the aortic root, each time with one of the three interactive modalities.

During the experiment, participants are prohibited from viewing the transparent phantom directly. Instead, they are asked to act upon visual feedback from either a standard 2D monitor or from a HoloLens. When wearing the HoloLens, participants have the flexibility to alter their positions during the experiment to view visual feedback from various angles. The procedure of a single trial can be outlined as follows:

1. both clamps of the catheter driver are released, and the catheter is positioned inside the catheter driver.
2. the catheter is advanced manually until its tip reaches the starting point of the planned path. To reduce friction, the catheter body is lubricated with baby oil.
3. the control system is initialized.
4. the user teleoperates the catheter. The task entails aligning the catheter tip with the predetermined trajectory until the end, following the sequence of green spheres one at a time. The user is suggested to follow the guidance provided by the yellow arrow, which indicates both the direction and degree of catheter bending required (by the length of the yellow arrow).
5. the duration of the procedure is recorded. Users are expected to complete the experiment within three minutes. If users feel they have not achieved the target accurately and there is still time remaining, they may decide to retract the catheter and attempt to target again.
6. the catheter is subsequently retracted to the starting point. This retraction is executed rapidly, without meticulous control.

In this experiment, the focus is exclusively on validating the insertion, which is deemed to be more challenging and safety-critical compared to retraction. During insertion, improper tip movement could potentially exert excessive force on the vessel walls. This may lead to either vessel rupture or dislodgment of calcifications. Both scenarios can be caused by the sharp tip of the catheter. The experiment was continuously monitored throughout its duration. If any accident would occur, such as users damaging the aortic phantom, the experiment would be halted immediately.

C. Performance Metrics

The performance metrics can be categorized into subjective and objective measures. Subjective evaluations are derived from questionnaires and the NASA-TLX form (introduced in Section III-A). The objective metrics that are used to quantify the performance will be introduced as follows.

For assessing clinical performance in endovascular interventions, several gold standards and other criteria are commonly employed by clinicians [37], including clinical outcomes, technical success, and safety. From an engineering perspective, previous studies [38], [39], [40] have aimed to objectively assess the skill levels of cardiologists by analyzing the kinematics of catheters, which involves extracting various features and metrics. In line with both types of evaluation methods previously described, our study incorporates the following specific performance metrics to comprehensively assess user performance of robotic catheterization in in-vitro environment:

1) Duration (T): The duration is defined as the time span from the initiation to the completion of a single experiment. It begins when the user starts teleoperating the robotic catheter, marked as t_0. The duration concludes when the catheter reaches the aortic root, and the user verbally confirms his (or her) satisfaction with the obtained targeting accuracy. This instant is marked as t_g. The duration T is then simply:

$$T = t_g - t_0 \tag{5}$$

Note that the maximum allowed time for each experiment is 3 minutes. If this limit is exceeded, the user is asked to repeat the trial.

2) Tracking Error (T_r): The tracking error refers to the average deviation between the actual trajectory $\boldsymbol{s_j}$ ($j = 1, \ldots k$ with $t = t_0$ when $j = 1$, and $t = t_g$ when $j = k$) and desired trajectory $\boldsymbol{s_i^d}$ ($i = 1, \ldots n$). In our experiments, the number of setpoints of the desired trajectory n is set to 500. These setpoints are interpolated from the output of the RL path planning algorithm, originally consisting of 26 setpoints. The actual trajectory is recorded by an EM sensor at a sampling frequency f of 40 Hz. For each point $\boldsymbol{s_j}$ on the actual trajectory, the shortest distance to the desired trajectory is identified and treated as the deviation for that individual point. The tracking error is computed as the mean error of all these individual points:

$$T_r = \frac{1}{k}\sum_{j=1}^{k}\left(\min_{\mathbf{i}}||\boldsymbol{s_i^d} - \boldsymbol{s_j}||\right) \tag{6}$$

Depth tracking error, denoted as T_{rz}, specifically quantifies the tracking error along the z-axis, representing the portion of error related to the depth direction. This parameter serves to determine whether the disparities in the tracking error arise predominantly from errors in the depth direction.

3) Targeting Error (T_a): The targeting error is calculated by searching the entire trajectory and determining the shortest distance between the trajectory $\boldsymbol{s_j}$ and the target $\boldsymbol{s_n^d}$. This metric serves as a criterion for evaluating the accuracy of reaching the target.

$$T_a = \min_{\mathbf{j}}||\boldsymbol{s_n^d} - \boldsymbol{s_j}|| \tag{7}$$

4) Total Path Length (L): The path length is determined as the summation of the Euclidean distances between consecutive trajectory points:

$$L = \sum_{j=1}^{k-1}||\boldsymbol{s_{(j+1)}} - \boldsymbol{s_j}|| \tag{8}$$

5) Dimensionless Squared Jerk (J_d): The smoothness of a trajectory can be measured as Dimensionless Squared Jerk (DSJ), which is designed to remain independent of both the total duration of an experiment and the amplitude of path length. The DSJ, introduced in [40], [41] and denoted as J_d, is mathematically expressed as:

$$J_d = \left(\frac{1}{3} \sum_{j=4}^{k} \left(\dddot{s}_{x,j}^2 + \dddot{s}_{y,j}^2 + \dddot{s}_{z,j}^2 \right) \Delta t \right) \times \frac{T^5}{L^2}$$

$$\text{where} \quad \dddot{s}_{a,j} = \frac{\ddot{s}_{a,j} - \ddot{s}_{a,j-1}}{\Delta t}$$

$$\ddot{s}_{a,j} = \frac{\dot{s}_{a,j} - \dot{s}_{a,j-1}}{\Delta t}$$

$$\dot{s}_{a,j} = \frac{s_{a,j} - s_{a,j-1}}{\Delta t} \tag{9}$$

Here, $\dddot{s}_{a,j}$ represents the third-order derivative of the trajectory $\boldsymbol{s_j}$ along the a-axis with respect to time t, for $a = x, y, z$. The total duration, denoted as T and defined in (5), and the total path length, denoted as L and defined in (8), are used to normalize the metric DSJ. Given the high values of DSJ observed in our study, the natural logarithm of DSJ is shown in figures and for comparative analysis.

The relationship between the employed evaluation metrics and the clinical performance in endovascular interventions is described as follows: Duration is a valuable indicator of procedure performance, particularly with regard to safety [42]. It not only impacts patient safety and comfort but also determines the availability of both the catheterization lab and clinicians. Tracking error serves as a measure of safety. A smaller tracking error indicates a trajectory closely aligned with the reference trajectory, reflecting a reduced risk of complications, such as vascular injury. Targeting error serves as a measure of the technical success of the procedure. A smaller targeting error reflects accurate device deployment. Total path length and DSJ are used to evaluate the smoothness of paths. Smoother paths can lead to faster procedures and less accidental contact with the vessel wall, thereby contributing to a safer procedure overall.

The significance of differences between interactive modalities is assessed through statistical tests. Because the selection of the significance test method differs based on the data distribution, the distribution of each data set was first examined to determine whether it follows a normal distribution, using the Shapiro–Wilk test [43] with a significance level of 0.05. Subsequently, depending on their respective characteristics, we applied the Kruskal-Wallis test [44] for populations that did not follow a normal distribution, and utilized the t-test [45] for those that were normally distributed. A significance level of 0.05 is used for both tests.

IV. Results and Discussion

A. User Profiles and Subjective Evaluation

Fifteen participants, aged between 20 and 35 years and with an educational background in engineering, participated in the user study. The user profiles are summarized in Fig. 6. Twelve out of fifteen, wear glasses, with three participants not requiring them. Thirteen participants are right-handed, while only two individuals are left-handed. Eight participants identified themselves as novices with no previous experience with the HoloLens. Four participants indicated to have an intermediate experience level, having used the HoloLens several times. Three participants are highly experienced, frequently using HoloLens as a part of their regular job duties. As for the gaming experience with a gamepad, three participants are novices, seven have an intermediate level of experience, and five are highly experienced. From the aforementioned statistics, it can be concluded that users have more experience with gamepad compared to HoloLens. This difference in experience may contribute to the varying levels of confidence when using these two control devices. Lastly, with regard to their experience with steerable catheters, nine participants have never steered a catheter before. Three participants possess some steerable catheter experience, and the remaining three participants interact with steerable catheters regularly.

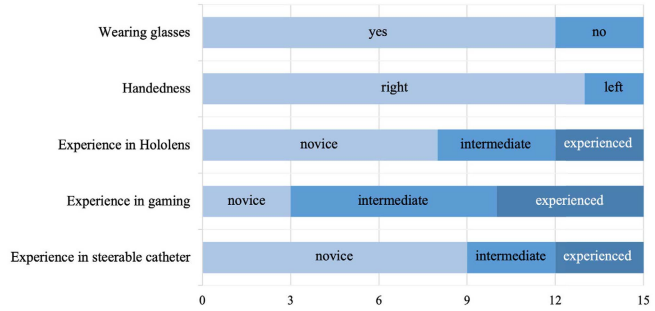

Fig. 6. Summary of the fifteen user profiles, detailing their gaming, HoloLens, catheter experience, handedness, and eyewear usage.

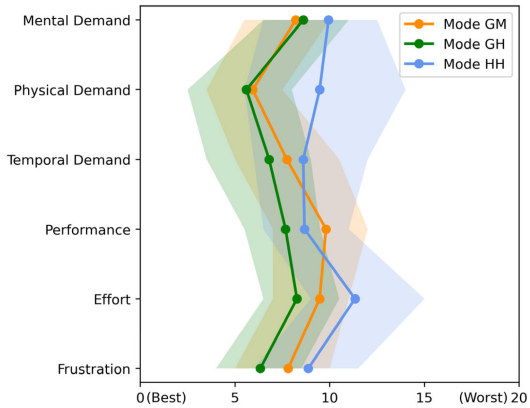

Fig. 7. NASA-TLX scores (20-scale) represent the workload associated with three interactive modalities. Note that lower scores indicate less workload perceived by the users.

The perceived workload measured via NASA-TLX form is depicted in Fig. 7. The central line illustrates the average score (20-scale) from fifteen users across the six different aspects of the NASA-TLX form. The colored area represents the interquartile range, with its boundaries indicating the lower and upper quartiles (i.e., 25% and 75%). It is important to note that a lower

score signifies less workload perceived by users, namely better performance.

1) Evaluation From NASA-TLX: Regarding mental demand, both Mode GM (scored at 8.2) and Mode GH (scored at 8.6) demonstrate similar performance levels, surpassing Mode HH, which scored 9.9. However, when considering physical demand, Mode GM and Mode GH significantly outperform Mode HH, suggesting that using HoloLens as input device requires more physical effort. This may be due to HoloLens users constantly holding their arms to maintain catheter control, concerned that dropping their arms might result in unrecognized hand gestures, a loss of control, and potential damage to the catheter or phantom. In contrast, gamepad users can rest their elbows at their waist and lower their hands to a more relaxed position, reducing physical strain. Regarding temporal demand, the modes operated with a gamepad (Mode GH and Mode GM) exhibit a marginal advantage over Mode HH. When using the HoloLens, some novice users tend to maintain a consistent catheter speed by placing speed control blocks in the same position and focus on controlling the catheter's bending, while expert and intermediate users typically possess a better knowledge of adjusting the catheter speed in response to the varying locations of the catheter tip. In contrast, all users, when using gamepad, more actively adjust the insertion speed to their liking. In easier-to-navigate areas, such as the descending aorta, users tend to select a higher speed. As a result, gamepad-based catheter control is generally faster than HoloLens-based control. The best performance is perceived as Mode GH (7.7), followed by Mode HH (8.7), and lastly Mode GM (9.8). This suggests that the 3D visual feedback from the HoloLens enhances user confidence. In terms of effort and frustration, Mode GH stands out as the most favorable, significantly outperforming Mode HH, with Mode GM ranking moderately between the two. This could be attributed to the fact that most users have more experience with gamepad than with HoloLens, making catheter control via gamepad easier for them. In the HoloLens scenario, users with limited experience may face challenges in achieving accurate hand recognition, especially when employing hand rays, a method used for interacting with holograms remotely. These issues primarily contribute to increased effort and potential frustration for users.

In subjective evaluations, Mode GH consistently outperforms the other two interactive modes, achieving an average score of 7.2 across six aspects. This represents a 12.2% reduction in performance compared to Mode GM, which scores 8.2, and a 24.2% reduction compared to Mode HH, with its higher score of 9.5. This suggests that using a gamepad for control and a HoloLens for visual feedback creates the most comfortable user experience. The standard deviations of Mode GM, GH, and HH are 3.8, 3.7, and 3.8, respectively, indicating that the difference in opinions among users is not large.

2) Results From Questionnaire: Users were asked to rank the three modes in descending order of preference. The outcomes of this preference ranking are presented in Fig. 8. Mode GH is the most preferred among users, with 67% selecting it as their first choice and 33% as their second choice. Compared to 10 out of 15 users who prefer Mode GH as their first choice, only 2 out of 15 users selected Mode GM, and 3 out of 15 chose Mode HH as their primary preference. Mode GM and HH exhibit comparable preference outcomes.

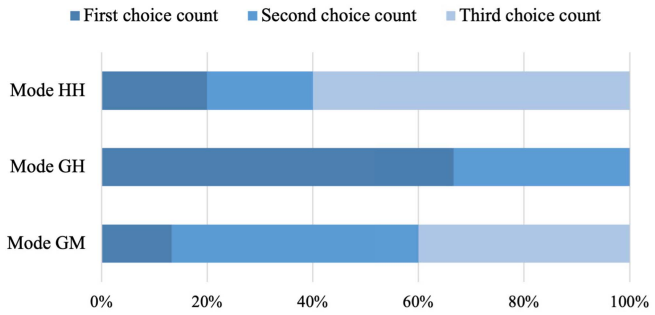

Fig. 8. User preference for three modes. The x-axis represents the percentage of users who selected the respective mode as their top preference, second preference, or third preference.

In the questionnaire, users were asked to share their likes and dislikes about the experiment, providing complementary insights into their NASA-TLX scores. For control, the gamepad is generally preferred due to users' familiarity and its ergonomic design. However, the limited bending angle of the thumbstick, combined with the control strategy that maps the thumbstick's bending angle to the pressure of the artificial muscles, causes users to perceive the gamepad as overly sensitive, making fine motion control challenging. This, however, may potentially be a limitation of the current implementation and is not necessarily a fundamental limitation of the interface. On the other hand, the HoloLens offers a larger panel for regulating the catheter bending, resulting in higher control resolution and facilitating easier and finer motion control compared to the gamepad. An additional comparative study with a Haption Virtuose robot as the control input device, which offers a larger range of motion, is detailed in Section V. The users reported that, when using the HoloLens, the primary concern is the potential inaccuracy of hand gesture recognition. This may stem from users' limited experience with the device. This can lead to anxiety over the possibility that the catheter might not stop and cause damage to the catheter tip or phantom due to excessive interaction force. Despite the availability of an emergency button, users remain apprehensive, as it also relies on hand gesture recognition.

In terms of visual feedback, users favor the HoloLens over a standard screen, as it displays 3D trajectories and allows users to move around the holographic phantom in the real-world space for more effective catheter tip alignment. In contrast, 2D screens do not offer depth perception. Users can manipulate the virtual model to view it from various angles, but this requires an input device and is challenging since their hands are already engaged with the gamepad. Moreover, this approach lacks the intuitiveness and efficiency of moving around the hologram directly with the HoloLens. Only one user reported dizziness from using the HoloLens.

In addition, users appreciate the HoloLens feature that allows easy relocation of holograms according to individual preferences. In our experiment, users differed in body height as well as their preferred placement for the holographic components. They

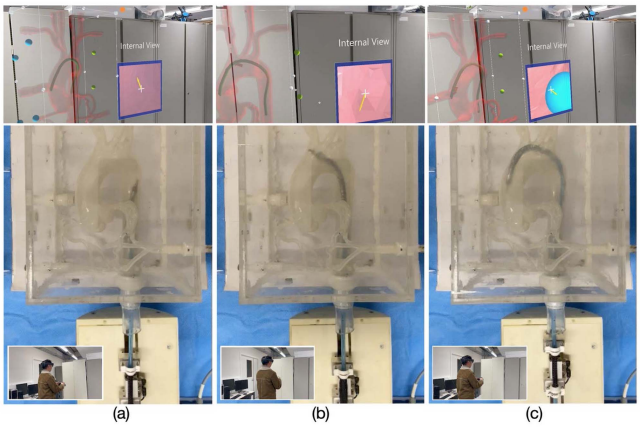

Fig. 9. Experimental procedure with the robotic catheter at three different locations when steering using Mode GH: a) descending aorta; b) aortic arch; c) aortic root.

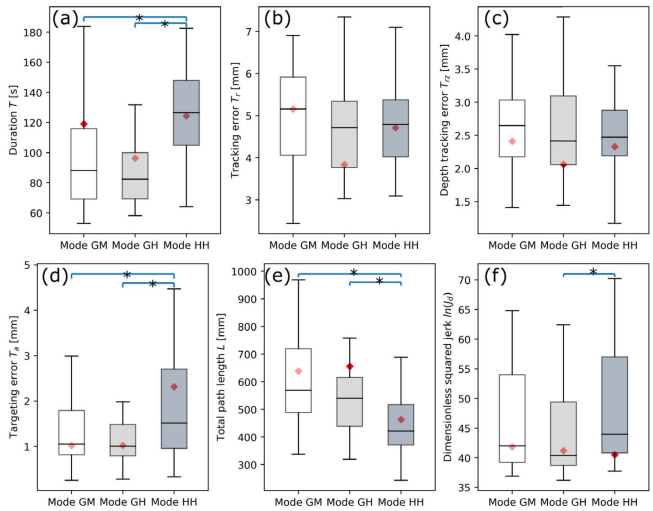

Fig. 10. Box plots depict (a) duration, (b) tracking error, (c) depth tracking error, (d) targeting error, (e) total path length, and (f) dimensionless squared jerk for the three interactive modalities, showing median, interquartile range, and data's minimum-maximum span. The red diamond represents the median value among users with an experienced level in HoloLens. A line labeled with an asterisk connecting two groups indicates a significant difference between them (i.e., $p < 0.05$ using Kruskal-Wallis test or t-test).

reported that they utilized the relocation feature to adjust the location of the control and visualization panel to their preference both prior to and during the experiment. However, there were instances where occasional modifications were executed during the experiment. This customization accommodates diverse user needs and enhances overall satisfaction. Conversely, for the gamepad, two users, who identified themselves as intermediate or experienced gamers, indicated a preference for an arrangement where bending control is assigned to the right thumbstick, and forward/backward movement to the left thumbstick, consistent with the design found in most computer games.

As for the investigation on the effectiveness of the internal view, 13 out of 15 users agreed that the internal view was beneficial during the procedure. Only one user chose the option "neither useful nor unuseful" and one user chose the option "unuseful" as he (she) relied entirely on the HoloLens' 3D visualization capabilities, and thus did not depend on the internal view at all.

B. Objective Evaluation

Fig. 9 illustrates the experimental procedure through three distinct stages. In Fig. 9(a), the catheter is positioned in the descending aorta, and the internal view features an arrow pointing towards the upper left. This informs the user that the catheter needs to start bending in that direction to follow the optimal path and to navigate through the aortic arch. Fig. 9(b) shows that the catheter is almost past the aortic arch, with the guidance arrow pointing towards the bottom left, indicating the need for increased bending by the increased length of the yellow guidance arrow. In Fig. 9(c), the catheter successfully reaches the aortic root, as demonstrated by the corresponding HoloLens view where the blue target is nearly achieved. An arrow pointing towards the bottom-right direction suggests that by gently bending the catheter in this direction, the target can be reached. During the entire user study, no damage to the aortic phantom was observed. For a comprehensive recording of the experimental procedure, please refer to the video.[1]

The data gathered during the experiment was analyzed to derive the performance metrics, as detailed in Section III-C. Fig. 10 illustrates the duration, tracking error, depth tracking error, targeting error, total path length, and dimensionless squared jerk for the three interactive modalities, achieved by the fifteen participants.

Regarding the tracking error, Mode GH displayed superior performance among all three interactive modes, with a median of 4.72 mm, followed by Mode HH (4.79 mm) and Mode GM (5.16 mm). Mode GH shows an improvement of 1.5% over Mode HH and 8.5% over Mode GM. Mode GM demonstrated the highest variance among the three modes, indicating considerable tracking performance disparities between users or trials, while Mode HH exhibited the lowest variance. These observations are in line with the results depicted in Fig. 11, which shows the full trajectories captured by the EM sensor for a single trial. It can be seen that Mode HH (Fig. 11(c)) has a less tortuous trajectory compared to Mode GM (Fig. 11(a) and (f)). This can be explained as follows: both control strategies (gamepad vs. HoloLens) establish a proportional relationship between the commands generated by the control input device and the pressure applied to the artificial muscle. In the HoloLens-based control, the green sphere for catheter control remains stationary upon release, resulting in a generally less tortuous trajectory. In contrast, the gamepad exhibits a spring effect, automatically returning to its neutral position when released. Consequently, improper control may produce a zigzag-shaped trajectory, as demonstrated in Fig. 11(f). Nevertheless, as depicted in Fig. 11(a), after multiple

[1]https://youtu.be/AR95oV6o9Ls

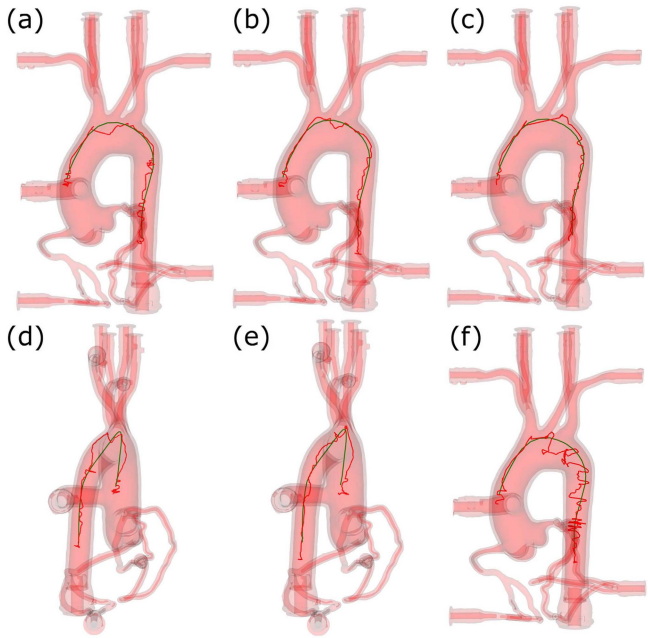

Fig. 11. Recorded trajectories of a single trial. (a) Mode GM; (b) Mode GH; (c) Mode HH; (d) side view of a; (e) side view of b; (f) another example in Mode GM with a zigzag-shaped trajectory due to improper control with the gamepad.

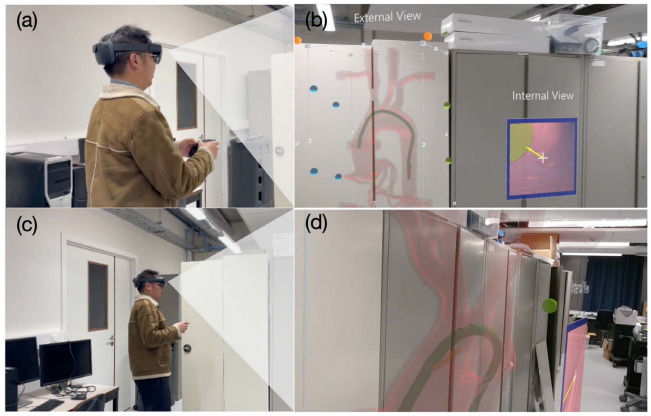

Fig. 12. The HoloLens enables users to see visual feedback from multiple perspectives: (a)–(b) users observe the holographic phantom from the front; (c)–(d) by physically maneuvering in the real world, users can observe the catheter tip from diverse angles, not just a frontal perspective.

trials, the gamepad-based control can also achieve a smooth trajectory and performance comparable to that of the HoloLens-based control. On the other hand, the gamepad-based control outperforms HoloLens-based control in terms of responsiveness and reliability. Maintaining consistent hand gesture recognition using HoloLens was found to be difficult for novices. This could be explained by the user feedback and the observations made during the user study: 1) users may not be familiar with the interacting principles of HoloLens, namely may not interact with holograms as if they were tangible objects. Consequently, when the hologram is not within the user's physically reachable range (i.e., limited by the length of arms), users sometimes still attempt to interact directly with the hologram; 2) users may not be fully accustomed to the HoloLens hand gesture command known as "air tap", which allows the user to pinch an object using the thumb and forefinger. During the study, some users attempted but did not manage to implement this gesture correctly, suggesting that they may not have fully exploited the opportunities for interaction with the hologram. In contrast to the HoloLens, the thumbsticks and buttons of the gamepad provide passive haptic feedback which is known to improve proprioception, which in turn may explain the gamepad's superiority compared to the HoloLens. Whereas in the HoloLens the user needs to visually confirm the input motion that was commanded, in a gamepad the user can rely on his/her proprioception to understand the pose and relative displacement of the input device. Conversely, the HoloLens, with its virtual interactive interface, requires users to maintain constant visual focus to accurately operate its objects.

Furthermore, it can be observed that the HoloLens significantly aids in reducing the tracking error, particularly in the depth direction (Fig. 11(d)–(e)). This is substantiated by the depth tracking error across the three interactive modes, as shown in Fig. 10(c). Mode GH and Mode HH exhibited comparable performance, with median errors of 2.42 mm and 2.47 mm, respectively. In contrast, Mode GM performed worse, registering an error of 2.65 mm. Fig. 11(d) and (e) display the side view of Fig. 11(a) (Mode GM) and Fig. 11(b) (Mode GH), respectively, with visual feedback provided by a standard 2D monitor and HoloLens. One can observe that their performance in the side view varies considerably. With HoloLens, the user effectively aligns the tip to the predefined trajectory in the side view. Conversely, on a 2D screen, the user may deviate from the trajectory in the side view, even if they believe that they have achieved satisfactory performance by solely confirming the frontal view. The results substantiate the benefits of HoloLens feedback, primarily when users move around the holographic phantom in real space, thereby viewing it from diverse angles. This user behavior is illustrated in Fig. 12. When paired with a gamepad, which offers high responsiveness and can be easily carried, optimal performance was achieved. On the other hand, this also suggests that there is room for improvement in the quality of 3D visualization; otherwise, users would not need to adjust their perspective by moving. In future research, we plan to implement an effective method for rotating the view displayed on the 2D screen and subsequently draw a comparison with the 3D visualization.

Regarding the targeting error, Mode GH exhibited the lowest error at 1.01 mm. Mode GM, with an error of 1.06 mm, outperformed Mode HH (1.52 mm). The significance test revealed statistically significant differences between Mode GH and Mode HH, as well as between Mode GM and Mode HH. The findings indicate that the gamepad demonstrates superior targeting ability compared to the HoloLens. When approaching the target, users can effortlessly halt the catheter driver's insertion, allowing ample time to modify the catheter tip's pose. Once prepared, they can advance the catheter driver, achieving the target rapidly. Conversely, when using the HoloLens as the input device, the majority of users find that halting the driver and adjusting the orientation of the tip necessitates synchronized movements of both the left and right hands. This involves handling hand gesture

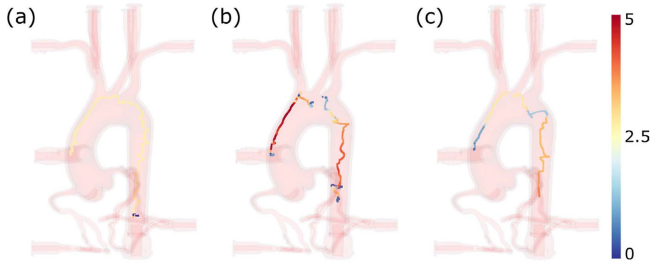

Fig. 13. Catheter insertion speeds (0–5 mm/s) in Mode HH, as performed by users with varying levels of experience with HoloLens, are depicted as follows: (a) novice user, (b) intermediate user, and (c) expert user.

recognition concurrently, which could be challenging given their limited familiarity with the HoloLens. As a result, they often attempt to target while the motion of catheter insertion is still ongoing, leading to increased targeting errors in Mode HH.

Concerning the duration, Mode GH (82.34 s) and Mode GM (88.10 s) demonstrated similar performance levels, with both being statistically distinct from Mode HH (126.53 s). This can be attributed to the ease of controlling the driver's speed using a thumbstick, as users can simply bend the thumbstick to adjust the speed. Stopping the driver is also straightforward, as users only need to release the thumbstick. On the other hand, when operating the system using the HoloLens, users frequently encounter challenges in dragging the slider back to the neutral region, where the speed is set to zero. Fig. 13 illustrates the varying catheter insertion speeds of users with different levels of experience in HoloLens, arranged from left to right as novice, intermediate, and expert users. The color heat map represents speed, with red indicating high speed, yellow representing medium speed, and blue symbolizing low speed. One can observe from the figure that a user's level of experience could impact his (her) steering style. Part of novice users adhere to a consistent and moderate speed of about 2.5 mm/s, directing their primary attention towards the control of bending maneuvers. Both the intermediate and the expert users demonstrate the ability to adjust their speeds flexibly according to different regions. In the descending aorta, where the vessel is nearly straight, some intermediate and expert users navigated at higher speeds. They choose to reduce their speeds when crossing the aortic arch. As shown in Fig. 13(b)–(c), users exhibit divergent behaviors when approaching the target. Some maintain high speeds, while others adopt a more cautious approach by slowing down the insertion speeds and adjusting the catheter tip's pose for improved targeting accuracy.

The total path length serves as a measure of the tortuosity or static smoothness of a trajectory. In this evaluation, Mode HH stands out for its superior performance, achieving a median path length of 420.98 mm. This is followed by Modes GH and GM, which show comparable results with median lengths of 539.62 mm and 569.30 mm, respectively. This disparity is mainly due to the gamepad's tendency for creating zigzag trajectories, a consequence of its lower control resolution and our specific control strategy. Interestingly, regarding the total path length in Mode HH, experienced HoloLens users follow longer trajectories as their total path length is larger than the median performance of all users. This phenomenon can be attributed to the fact that a shorter total path length is not always indicative of better performance. Often, more meticulous attempts to follow the trajectory can lead to an increased total path length. However, this observation warrants further validation in future research. Furthermore, the natural logarithm of the DSJ metric sheds light on the trajectory's dynamic smoothness, specifically the frequency of changes in the acceleration of the catheter motion in 3D. Here, Modes GM (42.01) and GH (40.38), both using gamepad controls, achieved lower values compared to Mode HH (43.95). This is a result of the limited bending range of the thumbstick on the gamepad, which often leads users to select either its neutral (0 mm/s) or maximum (5 mm/s) speed setting. In contrast, HoloLens-based control offers users a wider spectrum of speed options, facilitating control with more variable speeds.

The diamonds in Fig. 10 represent the median performance of the users who identify themselves as experienced HoloLens users. This representation allows for the analysis of the relationship between the users' HoloLens experience and their performance. Fig. 10(b) highlights that prior experience with HoloLens leads to a substantial reduction in tracking error, especially when the HoloLens is combined with a gamepad for control. In Mode GH, the reduction of tracking error amounts to 19.5% compared to the median of all other users in the same mode, and a 25.6% reduction compared to their own performance in Mode GM. A comparable trend is evident in the depth tracking error, exhibiting a decrease of 19.5% relative to the median of all other participants in the same interactive mode, Mode GH. However, in terms of targeting error, the medians of experienced users in Mode GH and Mode HH do not show reductions, suggesting that the HoloLens experience might not contribute to improvements in targeting error. For the other two metrics, namely duration and the DSJ in Mode HH, better performance is noted among users with a higher level of HoloLens experience. The results indicate a 1.8% decrease in duration and a 7.8% decrease in DSJ.

Overall, significant differences are observed in 4 out of 6 evaluation metrics between Mode GH and Mode HH, while Mode GM and Mode HH demonstrate significant differences in 3 out of 6 metrics. Although Mode GH and Mode GM do not exhibit significant differences, a trend is observable in 5 out of 6 metrics where Mode GH outperforms Mode GM, as evidenced by the smaller median value of Mode GH compared to Mode GM. To draw a more robust conclusion about the comparison between Mode GH and Mode GM, an analysis with a larger user base is envisioned in the future.

Fig. 14 illustrates the users' performance as a function of the number of trials to determine the presence of any learning curves. Fig. 14 features a combination of a violin plot [46] and a line plot. The violin plot is a method for visualizing the distribution of numerical data, combining a box plot with a kernel density estimation. The kernel density estimation is a statistical technique used to estimate the probability density function of a continuous random variable. In a violin plot, the width and shape of the violin at various points depict the data density at those locations, offering improved visualization of

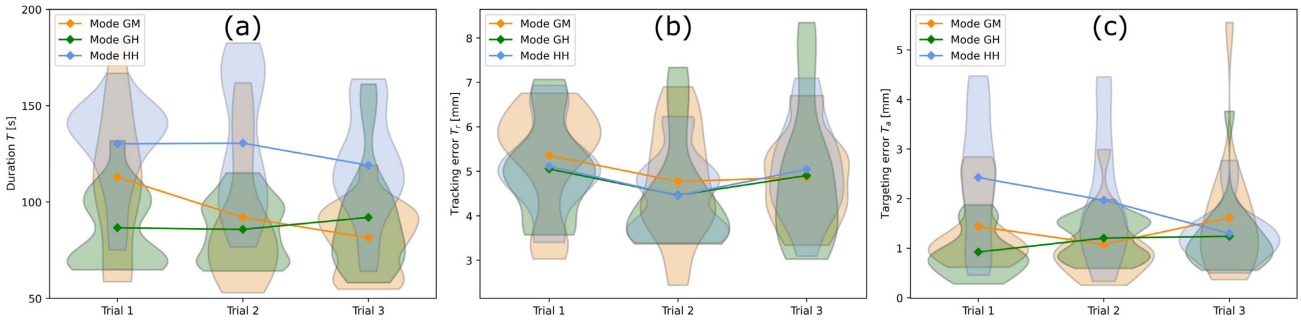

Fig. 14. User performance, as a function of the number of trials, is depicted using violin and line plots for comprehensive visualization.

data density across different values. The line plot is created by connecting the average values, which illustrates the trends in the learning process. Experimental duration demonstrates the most significant learning curve. For both Mode GM and Mode HH, the duration decreases considerably as the number of trials increases, as evidenced by both the line plot and data distribution. In the case of Mode GH, although the average duration in the third trial increases, the data distribution reveals that this is due to outliers substantially raising the average value. Most users complete their experiments in Mode GH within 120 s. The reason for the maximum duration of 164 s in trial 3 of Mode GH is that the user initially found the target performance unsatisfactory, leading him (her) to retract the catheter and make another targeting attempt. Regarding tracking error, a trend of initial decrease followed by a slight increase was observed in the three modes (see Fig. 14(b)). However, upon focusing on the distribution of the data, it is noted that the overall trend still indicates a decrease. In terms of targeting error, Mode HH exhibits the most pronounced learning curve. Additionally, the data distribution area narrows as the number of trials increases, indicating fewer outliers. In the third trial of Mode HH, all trials have an error of approximately 1 mm. In general, it is quite challenging to analyze the learning effects through just three trials. Future work should have an increased number of trials to better access the learning behavior.

To summarize, our findings can be outlined in the following bullet points, taking into account that only a limited number of participants were involved.

- the combination of a gamepad as a control input device and a HoloLens as a visualization device demonstrated the highest performance and user preference;
- compared to the HoloLens, the gamepad offers advantages such as familiarity from gaming, exceptional responsiveness (compared to hand gesture recognition of the HoloLens), tangible buttons that eliminate the constant need for visual attention, and ergonomic design enabling comfortable use;
- on the other hand, the HoloLens can provide high-resolution control for fine motions and the flexibility to reposition holographic control components on the spot;
- the HoloLens outperforms the 2D monitor by: a) displaying 3D images of the aortic phantom and catheter position in the user's view, offering a 360-degree interactive environment with depth perception, and b) allowing hands-free interaction with holographic models, eliminating the need for a mouse, keyboard, or gamepad as required with a 2D monitor.

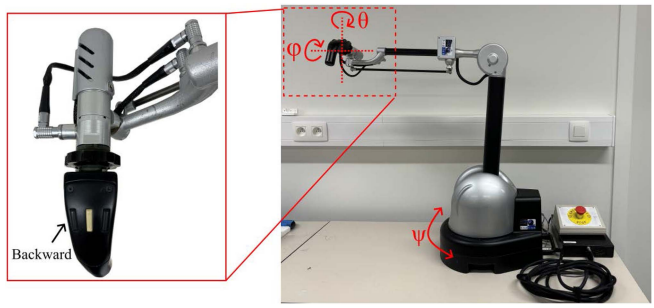

Fig. 15. Schematic representation of control input commands using the Haption Virtuose 6D RV robot. The right image illustrates the three DoFs used to command the translation and bending of the catheter, while the left image provides a close-up of the handle.

V. Additional Study With Haption Virtuose Robot as a Control Input Device

In the previous section, a gamepad was used as the control input device for steering the catheter. However, as noticed by experts in the fields as well as by participants of the study, the gamepad offers only a limited range of motion which may be suboptimal, rendering catheter steering unnecessarily challenging. Therefore, this section investigates the use of an alternative control input device with a larger range of motion, comparing its performance with that of a gamepad.

The Haption Virtuose 6D RV robot (Haption Inc., France) was utilized as another control input device in this study (see Fig. 15). This robot, featuring a large workspace, offers a potential solution to the limitations encountered with the gamepad. The robot has 6 DoFs, which allows it to coordinate the catheter control with a single hand. Prior to each use, the Haption Virtuose 6D RV robot requires a calibration. This is achieved by pressing the designated "force feedback" calibration button located on the robot. This action prompts all the robot's joints to move to their physical limit positions, after which the robot's joint angles are accurately reset to predefined neutral positions. These positions serve as the baseline from which all subsequent movements are precisely measured and executed.

TABLE IV
COMPARISON OF PERFORMANCE BETWEEN MODE VH AND MODE GH, PRESENTED AS MEAN ± STANDARD DEVIATION

	Mode GH	Mode VH	Mode VH
No. trials	1st - 3rd	1st - 3rd	4th - 6th
T [s]	143.46 ± 23.62	119.41 ± 16.89	143.32 ± 23.43
T_r [mm]	3.20 ± 0.25	2.83 ± 0.36	2.87 ± 0.32
T_{rz} [mm]	1.89 ± 0.20	1.71 ± 0.20	1.61 ± 0.22
T_a [mm]	0.77 ± 0.73	2.08 ± 1.10	0.80 ± 0.18
L [mm]	571.58 ± 31.98	349.18 ± 23.45*	380.41 ± 56.30*
$ln(Jd)$	41.72 ± 0.74	47.10 ± 4.89	44.67 ± 5.37

Note: The value labeled with an asterisk indicates a significant difference between this mode and the Mode GH (i.e., $p < 0.05$ using Kruskal-Wallis test or t-test).

The rotation angle of the base ψ, being the first joint, was utilized to linearly control the velocity v of the catheter driver as shown in (10). A button on the robot handle was used to swap motion direction and retract the catheter. Furthermore, the pitch and yaw angles of the handle (ϕ, θ) were proportionally mapped to the pressure values sent to the four PAMs of the catheter, thereby enabling control of the spatial bending of the catheter.

$$v \propto \beta\psi \text{ and } \beta = \begin{cases} 1 & \text{if Backward button OFF} \\ -1 & \text{if Backward button ON} \end{cases} \tag{10}$$

As Mode GH demonstrated superior performance among the three modes evaluated, this additional study focuses exclusively on the combination of the Haption Virtuose robot as the control input device and the HoloLens for visualization (referred to as Mode VH henceforth). A proficient user, experienced in both HoloLens and steerable catheter operation and who was also among the 15 participants in the user study, took part in the additional study. The user conducted six trials in Mode VH, which were then compared to the same user's three trials in Mode GH. The experimental procedure, task details, and performance metrics employed are consistent with those described in Section III. For an example of the experimental procedure, please consult the video.[2]

Table IV compares the performance in Mode VH (across six trials) with the user's performance in Mode GH (across three trials). To mitigate any learning effect due to the higher number of trials in Mode VH, these six trials will be divided into two groups: the 1st-3 rd trials and the 4th-6th trials (shown in the last two columns in Table IV), for a more fair comparison. The values in the last two columns of Table IV that are labeled with an asterisk indicate a significant difference between this mode and Mode GH. If the first three trials of Mode VH are compared to Mode GH, one can observe that the Virtuose-based control significantly outperforms the gamepad-based control in terms of total path length, achieving a reduction of 38.9%, with statistical significance observed between the two modes. Fig. 16 illustrates that the path taken with Virtuose-based control is less tortuous compared to that with gamepad-based control. The extended motion range of the Virtuose robot facilitates finer motion and adjustment, enabling more precise adherence to the intended target path. Additionally, the average tracking error decreased from 3.20 mm in Mode GH to 2.83 mm in Mode VH.

[2]https://youtu.be/4no3LYR0CZ4

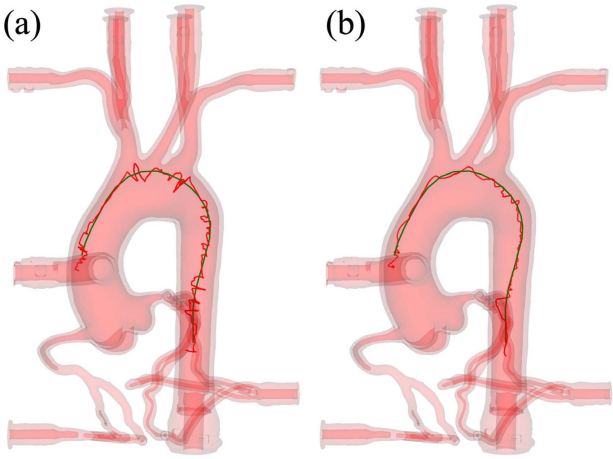

Fig. 16. The recorded trajectories of a single trial: (a) Mode GH; (b) Mode VH.

The duration and dimensionless squared jerk are comparable between the two modes. Mode VH shows a larger targeting error compared to Mode GH, suggesting that for tasks demanding precise targeting, using both hands for control may be easier than relying on one-handed control, which necessitates coordinated motion. However, this inference requires validation with a larger pool of users. Furthermore, by comparing the results of the 4th-6th trials with the 1st-3 rd trials in Mode VH, one can observe that apart from targeting error, the learning effect is not significant. The decrease in average targeting error from 2.08 mm to 0.80 mm demonstrates that with adequate training, Virtuose-based control can achieve results comparable to gamepad-based control in a targeting task. However, it is observed that the Virtuose robot restricts users to a fixed location during the procedure, resulting in the loss of hands-free interaction with holographic images.

It is important to note that the study of Mode VH in this paper serves as a supplementary investigation. It aims to validate whether a control input device, such as the Haption robot with a larger range of motion, could contribute to a smoother trajectory. Meanwhile, the main focus of this paper remains the comparison between Modes GH, GM, and HH. We acknowledge that more conclusive findings in Mode VH can only be obtained through the involvement of additional users and plan to address this in future work.

VI. CONCLUSION

Fluoroscopy has been crucial for catheterization procedures, yet it exhibits certain limitations. Firstly, it is unable to provide depth perception. Secondly, fluoroscopy is associated with ionizing radiation. To address these challenges, employing teleoperation for catheter steering and using 3D visualization devices could provide substantial benefits.

In this article, three interactive modes using distinct control and visualization devices are compared through a user study. An endovascular robotic system, comprising a robotic catheter, HoloLens, and a gamepad, is constructed for experimental validation. It is revealed by the user study that the greatest

appreciation and performance are achieved for the combination of gamepad as the control device and HoloLens as the visualization device. By moving within the physical space, users can explore various perspectives of holographic imaging through the HoloLens. The gamepad, on the other hand, is recognized as an easy-to-use and intuitive control device that is highly responsive and portable. The study has been extended to include the use of the Haption Virtuose robot as a control input device, examining whether a larger range of motion in such a device can enhance performance. The results revealed that paths navigated using Virtuose-based control were less tortuous than those achieved with gamepad-based control, while other evaluation metrics showed similar performance levels. In the future, it would be advantageous to conduct a user study that focuses on Virtuose-based control, which could compare the efficacy of single-handed coordination versus two-handed coordination.

The findings of this user study hold the potential to improve current endovascular interventions by introducing an innovative clinical workflow. In this approach, physicians remotely maneuver the catheter using a gamepad while wearing a HoloLens. Within the HoloLens, a holographic representation of the anatomy is superimposed onto the patient's body. The catheter's configuration, such as tip position and shape, can be acquired through non-radiative methods such as EM tracking or Fiber Bragg Grating (FBG) sensing and subsequently represented in the holographic anatomy. Guided by AR, physicians could potentially navigate catheters and guidewires using an intuitive teleoperation approach.

Validation of the impact of AR and teleoperation in an in-vitro vessel navigation study remains difficult owing to the limited availability of robust steerable catheter systems, the recent availability of high-quality AR HMD as well as the complexity of integrating these components. Despite these challenges, we have integrated these components and devised an AR interface, which results in a robotic catheterization system capable of operating in various interactive modes. In this study, the guidance cues are uniformly implemented across both 2D and 3D visualization methods. Therefore, the comparison purely lies in the distinctive characteristics of 2D and 3D visualization. For a more comprehensive understanding, additional studies are required on different types of guidance cues. Another limitation of this paper is the limited number of trials per user conducted so far. Given the delicate and complex structure of vessels, intuitive catheter steering becomes crucial in these applications. Therefore, it would be valuable to conduct an increased number of trials per user and engage a broader range of participants, including clinicians, in future research. Additionally, it would be advantageous to extend this investigation to in-vivo animal experiments.

Acknowledgments

The authors extend their deepest gratitude to the three anonymous reviewers for their extensive and meticulously detailed comments. The depth and scope of their feedback were instrumental in enhancing the quality of our paper. Additionally, we wish to express our appreciation to Omar AI-Ahmad for his expert assistance with the catheter driver. Special thanks also go to Jerome Perret from Haption S.A., Jef de Smet, Yuyu Cai for their valuable advice and insights regarding the Haption Virtuose robot.

References

[1] B. Ramlawi, "The era of catheter-based and minimally invasive cardiac surgery," *Methodist DeBakey Cardiovasc. J.*, vol. 12, no. 1, 2016, Art. no. 3.
[2] N. Z. Elgharib, U. H. Shah, and J. T. Coppola, "Transradial cardiac catheterization and percutaneous coronary intervention: A review," *Coronary Artery Dis.*, vol. 20, no. 8, pp. 487–493, 2009.
[3] J. Liu et al., "An augmented reality system for image guidance of transcatheter procedures for structural heart disease," *PLoS One*, vol. 14, no. 7, 2019, Art. no. e0219174.
[4] M. C. Palumbo et al., "An easy and user independent augmented reality based navigation system for radiation-free interventional procedure," in *Proc. IEEE Int. Symp. Med. Robot.*, 2022, pp. 1–7.
[5] V. García-Vázquez et al., "Navigation and visualisation with HoloLens in endovascular aortic repair," *Innov. Surg. Sci.*, vol. 3, no. 3, pp. 167–177, 2018.
[6] C. A. Linte, J. Moore, A. Wiles, J. Lo, C. Wedlake, and T. M. Peters, "In vitro cardiac catheter navigation via augmented reality surgical guidance," in *Medical Imaging 2009: Visualization, Image-Guided Procedures, and Modeling*, vol. 7261. Bellingham, WA, USA: SPIE, 2009, pp. 231–239.
[7] P. S. Batra, M. W. Ryan, R. Sindwani, and B. F. Marple, "Balloon catheter technology in rhinology: Reviewing the evidence," *The Laryngoscope*, vol. 121, no. 1, pp. 226–232, 2011.
[8] B. C. Clark et al., "Getting to zero: Impact of electroanatomical mapping on fluoroscopy use in pediatric catheter ablation," *J. Interventional Cardiac Electrophysiol.*, vol. 46, pp. 183–189, 2016.
[9] C. M. Stahl, Q. C. Meisinger, M. P. Andre, T. B. Kinney, and I. G. Newton, "Radiation risk to the fluoroscopy operator and staff," *Amer. J. Roentgenol.*, vol. 207, no. 4, pp. 737–744, 2016.
[10] S. Li, Z. Du, and H. Yu, "A robot-assisted spine surgery system based on intraoperative 2D fluoroscopy navigation," *IEEE Access*, vol. 8, pp. 51 786–51 802, 2020.
[11] Y. Zhang, L. Zhao, and S. Huang, "Aortic 3D deformation reconstruction using 2D X-ray fluoroscopy and 3D pre-operative data for endovascular interventions," in *Proc. IEEE Int. Conf. Robot. Automat.*, 2020, pp. 2393–2399.
[12] P. Ambrosini et al., "A hidden Markov model for 3D catheter tip tracking with 2D X-ray catheterization sequence and 3D rotational angiography," *IEEE Trans. Med. Imag.*, vol. 36, no. 3, pp. 757–768, Mar. 2017.
[13] E. K. Grant et al., "X-ray fused with MRI guidance of pre-selected transcatheter congenital heart disease interventions," *Catheterization Cardiovasc. Interv.*, vol. 94, no. 3, pp. 399–408, 2019.
[14] M. U. Farooq, A. Khasnis, A. Majid, and M. Y. Kassab, "The role of optical coherence tomography in vascular medicine," *Vasc. Med.*, vol. 14, no. 1, pp. 63–71, 2009.
[15] R. Loffroy et al., "Intravascular ultrasound in the endovascular treatment of patients with peripheral arterial disease: Current role and future perspectives," *Front. Cardiovasc. Med.*, vol. 7, 2020, Art. no. 551861.
[16] Y. Ma et al., "Cardiac unfold: A novel technique for image-guided cardiac catheterization procedures," in *Proc. 3rd Int. Conf. Inf. Process. Comput.-Assist. Interv.*, Springer, 2012, pp. 104–114.
[17] E. Bruckheimer et al., "Computer-generated real-time digital holography: First time use in clinical medical imaging," *Eur. Heart J.-Cardiovasc. Imag.*, vol. 17, no. 8, pp. 845–849, 2016.
[18] C. Diaz, M. Walker, D. A. Szafir, and D. Szafir, "Designing for depth perceptions in augmented reality," in *Proc. IEEE Int. Symp. Mixed Augmented Reality*, 2017, pp. 111–122.
[19] M. Benmahdjoub, A. Thabit, M.-L. C. van Veelen, W. J. Niessen, E. B. Wolvius, and T. Van Walsum, "Evaluation of AR visualization approaches for catheter insertion into the ventricle cavity," *IEEE Trans. Vis. Comput. Graphics*, vol. 29, no. 5, pp. 2434–2445, May 2023.
[20] S. Li, J. Cui, A. Hao, S. Zhang, and Q. Zhao, "Design and evaluation of personalized percutaneous coronary intervention surgery simulation system," *IEEE Trans. Vis. Comput. Graphics*, vol. 27, no. 11, pp. 4150–4160, Nov. 2021.
[21] T. Khan et al., "Understanding effects of visual feedback delay in AR on fine motor surgical tasks," *IEEE Trans. Vis. Comput. Graphics*, vol. 29, no. 11, pp. 4697–4707, Nov. 2023.

[22] M. Krichenbauer, G. Yamamoto, T. Taketom, C. Sandor, and H. Kato, "Augmented reality versus virtual reality for 3D object manipulation," *IEEE Trans. Vis. Comput. Graphics*, vol. 24, no. 2, pp. 1038–1048, Feb. 2018.
[23] N. Feizi, M. Tavakoli, R. V. Patel, and S. F. Atashzar, "Robotics and AI for teleoperation, tele-assessment, and tele-training for surgery in the era of COVID-19: Existing challenges, and future vision," *Front. Robot. AI*, vol. 8, 2021, Art. no. 610677.
[24] K. Wang et al., "Endovascular intervention robot with multi-manipulators for surgical procedures: Dexterity, adaptability, and practicability," *Robot. Comput.-Integr. Manuf.*, vol. 56, pp. 75–84, 2019.
[25] D. Filgueiras-Rama et al., "Remote magnetic navigation for accurate, real-time catheter positioning and ablation in cardiac electrophysiology procedures," *J. Vis. Experiments*, no. 74, 2013, Art. no. e3658.
[26] B. Rosa et al., "Intuitive teleoperation of active catheters for endovascular surgery," in *Proc. IEEE/RSJ Int. Conf. Intell. Robots Syst.*, 2015, pp. 2617–2624.
[27] C. J. Payne, H. Rafii-Tari, and G.-Z. Yang, "A force feedback system for endovascular catheterisation," in *Proc. IEEE/RSJ Int. Conf. Intell. Robots Syst.*, 2012, pp. 1298–1304.
[28] R. Erbel and H. Eggebrecht, "Aortic dimensions and the risk of dissection," *Heart*, vol. 92, no. 1, pp. 137–142, 2006.
[29] A. Devreker et al., "Fluidic actuation for intra-operative in situ imaging," in *Proc. IEEE/RSJ Int. Conf. Intell. Robots Syst.*, 2015, pp. 1415–1421.
[30] O. Al-Ahmad, M. Ourak, J. Vlekken, and E. V. Poorten, "Force control with a novel robotic catheterization system based on braided sleeve grippers," *IEEE Trans. Med. Robot. Bionics*, vol. 5, no. 3, pp. 602–613, Aug. 2023, doi: 10.1109/TMRB.2023.3291026.
[31] M. Quigley et al., "ROS: An open-source robot operating system," in *Proc. ICRA Workshop Open Source Softw.*, 2009, Art. no. 5.
[32] B. Nicoll, B. Keogh, B. Nicoll, and B. Keogh, *The Unity Game Engine and the Circuits of Cultural Software*. Berlin, Germany: Springer, 2019.
[33] K. S. Arun, T. S. Huang, and S. D. Blostein, "Least-squares fitting of two 3D point sets," *IEEE Trans. Pattern Anal. Mach. Intell.*, vol. PAMI-9, no. 5, pp. 698–700, Sep. 1987.
[34] Z. Li et al., "Robust path planning via learning from demonstrations for robotic catheters in deformable environments," 2024, *arXiv: 2402.00537*.
[35] K. U. Leuven, Research ethics - SMEC - documents and guidance, 2023. [Online]. Available: https://research.kuleuven.be/en/integrity-ethics/ethics/committees/smec/documents-and-guidance-for-your-application
[36] S. G. Hart and L. E. Staveland, "Development of NASA-TLX (task load index): Results of empirical and theoretical research," in *Advances in Psychology*, vol. 52. Amsterdam, The Netherlands: Elsevier, 1988, pp. 139–183.
[37] E. C. Saricilar, A. Freeman, and A. Burgess, "Evaluation of tools to assess operative competence in endovascular procedures: A systematic review," *ANZ J. Surg.*, vol. 91, no. 9, pp. 1682–1695, 2021.
[38] C. Duran, S. Estrada, M. O'Malley, A. B. Lumsden, and J. Bismuth, "Kinematics effectively delineate accomplished users of endovascular robotics with a physical training model," *J. Vasc. Surg.*, vol. 61, no. 2, pp. 535–541, 2015.
[39] S. Estrada, M. K. O'Malley, C. Duran, D. Schulz, and J. Bismuth, "On the development of objective metrics for surgical skills evaluation based on tool motion," in *Proc. IEEE Int. Conf. Syst. Man Cybern.*, 2014, pp. 3144–3149.
[40] E. B. Mazomenos et al., "Catheter manipulation analysis for objective performance and technical skills assessment in transcatheter aortic valve implantation," *Int. J. Comput. Assist. Radiol. Surg.*, vol. 11, pp. 1121–1131, 2016.
[41] N. Hogan and D. Sternad, "Sensitivity of smoothness measures to movement duration, amplitude, and arrests," *J. Motor Behav.*, vol. 41, no. 6, pp. 529–534, 2009.
[42] M. J. Yeh, E. Lydon, K. Gauvreau, K. J. Jenkins, D. Slater, and L. Bergersen, "Exploring procedure duration and risk for serious adverse events during congenital cardiac catheterization," *BMJ Surg., Interv., Health Technol.*, vol. 5, no. 1, 2023, Art. no. e000142.
[43] S. S. Shapiro and M. B. Wilk, "An analysis of variance test for normality (complete samples)," *Biometrika*, vol. 52, no. 3/4, pp. 591–611, 1965.
[44] P. E. McKight and J. Najab, "Kruskal-Wallis test," in *The Corsini Encyclopedia of Psychology*. Hoboken, NJ, USA: Wiley, 2010, pp. 1–1.
[45] B. L. Welch, "The generalization of 'student's' problem when several different population varlances are involved," *Biometrika*, vol. 34, no. 1/2, pp. 28–35, 1947.
[46] J. L. Hintze and R. D. Nelson, "Violin plots: A box plot-density trace synergism," *Amer. Statistician*, vol. 52, no. 2, pp. 181–184, 1998.

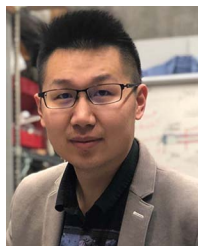

Di Wu (Graduate Student Member) received the MSc degree from the Technical University of Munich (TUM), Germany and the dual PhD degrees from KU Leuven, Belgium, and Delft University of Technology, the Netherlands, completed as part of Marie Skłodowska-Curie ATLAS Project under the European Union Innovative Training Network. He is currently a postdoctoral research associate with KU Leuven since 2023. He has also been a visiting graduate researcher with the Laboratory for Computational Sensing and Robotics (LCSR), Johns Hopkins University, USA, and The BioRobotics Institute of Sant'Anna School of Advanced Studies, Italy. One of his first-authored papers received Honorable Mentions for the Best Paper Award from IEEE Robotics and Automation Letters in 2021, and another was a finalist for the Best Paper Awards at IEEE-ISMR in 2019. His research interests include surgical robotics, robot control, and machine learning.

Zhen Li (Member, IEEE) received the BEng degree in intelligent science and technology from Nankai University, China, in 2017 and the dual MSc degrees in european master on advanced robotics (EMARO+) from the Warsaw University of Technology, Poland, and Ecole Centrale de Nantes, France, in 2019, and the dual PhD degrees in bioengineering and biomechanical engineering from Politecnico di Milano, Italy, and the Delft University of Technology, the Netherlands, in 2023 respectively, as an ESR with Marie Skłodowska-Curie ATLAS project under the European Union Innovative Training Network.

Mohammad Hasan Dad Ansari received the MSc in mechanican engineering from ETH Zurich and the joint PhD degree in biorobotics and engineering technology from Scuola Superiore Sant'Anna and KU Leuven. Since 2023, he is with the BioRobotics Institute of Scuola Superiore Sant'Anna in the Surgical Robotics and Allied Technologies area. Currently, his research activities are related to surgical robotics, worm-inspired robotics, and magnetic actuation.

Xuan Thao Ha received the MSc degree in systems, control and information technologies from Université Grenoble Alpes, France, in 2018. He is currently working toward the dual PhD degrees with the KU Leuven, Belgium, and the Sant'Anna School of Advanced Studies, Italy, with Marie Skłodowska-Curie ATLAS Project under the European Union Innovative Training Network. He also works with the Robot-Assisted Surgery (RAS) Group, Mechanical Engineering Department, KU Leuven. His research interests include surgical robotic, robot control, and sensing technology.

Mouloud Ourak received the MS degree in robotics and vision from Université de Montpellier, France, in 2013, and the PhD degree in automation from the Universit de Franche-Comt in 2016. Since 2017, he has been a postdoctoral researcher with the RAS Group, PMA Department, Katholieke Universiteit Leuven, Leuven, Belgium. His research interests include surgical micro-robotics (actuators and control laws) and visual servoing.

Jenny Dankelman (Member, IEEE) received the graduation degree in system and control engineering from the University of Groningen in 1984 and the PhD degree from the Delft University of Technology in 1989. She is professor in Minimally Invasive Surgery and Interventional Techniques (MISIT) with the Delft University of Technology. In 2001 she was awarded the Antoni van Leeuwenhoek chair and shortly after she became head of MISIT group. She cooperates with several hospitals such as Leiden UMC, Erasmus MC Rotterdam and University Medical Center Amsterdam. She was awarded the Royal award of Knight in the Order of Netherlands Lion and in 2019 she became member of Royal Netherlands Academy of Arts and Sciences.

Arianna Menciassi (Fellow, IEEE) received the graduation degree in physics from the University of Pisa in 1995 and the PhD degree from Scuola Superiore Sant'Anna (SSSA) in 1999. Since 2014, she has been a visiting professor in different universities in France, such as Pierre and Marie Curie and Besancon University. Since 2018, she has been the co-ordinator of the PhD in The BioRobotics Institute and she is a team leader of the "Surgical Robotics & Allied Technologies" Area. She was appointed as the vice-rector of the SSSA in 2019. She is a professor of Bioengineering and Biomedical Robotics with the SSSA.

Elena De Momi (Senior Member, IEEE) received the MSc degree in biomedical engineering in 2002, and the PhD degree in bioengineering in 2006, currently is assistant professor of Politecnico di Milano. From 2016, she has been an associated editor of IEEE ICRA, IROS and BioRob, area chair of MICCAI and she is currently Publication co-chair of ICRA 2023. She is PI for POLIMI of the EDEN2020 project and of ATLAS project and co-PI of the ARTERY project. She has been evaluator and reviewer for the European Commission in FP6, FP7, and H2020.

Emmanuel Vander Poorten (Member, IEEE) received the mechanical engineering degree from KU Leuven in 2000 and the title of doctor in engineering, from Kyoto University, Japan in 2007. He is associate professor with the Faculty of Engineering Technology of KU Leuven (Belgium) where, since 2010, he has been coordinating the activities of the Robot-Assisted Surgery (RAS) group. He has been heavily involved in several projects: RADHAR, SCATh, CASCADE, ARTERY, EurEyeCase, and ATLAS.